# Diffusiophoretic separation of colloids in microfluidic flows

Cite as: Phys. Fluids 32, 101302 (2020); doi: 10.1063/5.0023415 Submitted: 29 July 2020 · Accepted: 16 September 2020 ·







**Published Online: 13 October 2020** 

Sangwoo Shin<sup>a)</sup>

# **AFFILIATIONS**

Department of Mechanical Engineering, University of Hawaii at Manoa, Honolulu, Hawaii 96822, USA

Note: This paper is part of the Special Topic, Fluid-Structure Interactions: From Engineering to Biomimetic Systems.

al Author to whom correspondence should be addressed: sangwoos@hawaii.edu

#### **ABSTRACT**

In this review, we cover recent advances in microfluidic colloid separation enabled by diffusiophoresis. Diffusiophoresis describes the motion of colloidal particles induced by local chemical gradients. Despite its long history, it is only recently that diffusiophoresis has gained a renewed interest in the scientific community. Such a resurgence is, in part, due to the recognition that diffusiophoresis may enable useful applications that are otherwise difficult to achieve or can be augmented by it. One example is continuous colloid separation, which requires the control of particle motion relative to the flow. This review aims to provide a fundamental understanding of diffusiophoretic separation along with a survey of the recent literature on diffusiophoretic colloid separation in microfluidic flows in both cross-gradient and counter-gradient settings.

Published under license by AIP Publishing. https://doi.org/10.1063/5.0023415

# I. INTRODUCTION

Colloid separation plays a key role in numerous industrial processes and applications that are indispensable to our lives, such as water treatment, drug production, disease detection and prevention, personal care products, and food processing. In the past few decades, we have witnessed a surge of separation research enabled by microfluidics as it offers easy manipulation and visualization of fluids and particles, allowing for deeper understanding of existing systems as well as investigation of new separation processes.

Microfluidic separations require various external forces to direct the motion of colloidal particles relative to the flow. Available forces include electrostatic coulomb (electrophoresis), magnetic (magnetophoresis), dielectric (dielectrophoresis), thermal (thermophoresis), surface tension (tensiophoresis), sosmotic (diffusiophoresis), acoustic (acoustophoresis), optical (optophoresis), to and inertial forces (inertial migration). 11 While all of these mechanisms have certain pros and cons for separation purposes, diffusiophoresis offers distinct advantages, particularly over electrical methods that are widely used in biological and biomedical applications. Electrical separation methods such as electrophoresis and dielectrophoresis are inevitably associated with electrodes, power supplies, and bulky peripherals and often have the risk of inducing solvent electrolysis; diffusiophoresis is free from all of these downsides and thus potentially suitable for portable, wireless, and point-of-care diagnostics platforms.

Diffusiophoresis, which refers to the chemotactic migration of colloids induced by local chemical gradients, was first discovered by Derjaguin in the 1940s<sup>12</sup> and further established by Anderson and Prieve in the 1980s. <sup>13,14</sup> Aside from utilizing diffusiophoresis for enabling self-propelled microswimmers as a means to study active matter (self-diffusiophoresis or "active diffusiophoresis"), 15,16 has been growing interest in the area of "passive diffusiophoresis" in the past decade in which the motion of passive colloidal particles (e.g., homogeneous latex particles, liquid drops, <sup>17,18</sup> proteins, <sup>19,20</sup> DNAs, <sup>21,22</sup> cells, <sup>23,24</sup> and lipid vesicles <sup>25,26</sup>) is induced by externally imposed solute gradients. To get a broader sense of passive diffusiophoresis, refer to the seminal review article by Anderson, <sup>27</sup> as well as other excellent review articles published recently. 28-30 A number of unique observations have been made lately where diffusiophoresis was recognized to play an important role in several processes such as colloid stratification during drying,<sup>31</sup> colloidal self-assembly,<sup>32</sup> membrane fouling,<sup>33</sup> pattern formation,<sup>17</sup> fabric cleaning,<sup>34</sup> detection and healing of bone fractures, 35 cellular transport, 36,37 possibly the origin of life.

In terms of applications, there have been a fairly large number of diffusiophoresis studies dedicated to colloid separation in the past few years due to its promising aspects in separation processes. In this

review, we present recent advances in the diffusiophoretic separation of colloidal particles in microfluidic flows. Flows in colloidal separation systems commonly exist either parallel or perpendicular to the force field (e.g., concentration gradients). In general, microfluidic flows perpendicular to the force field are found mostly in continuous separation (sorting) systems, <sup>39,40</sup> whereas flows parallel to the force field are used for (pre)concentration purposes. 41,42 We first provide a brief introduction to colloid diffusiophoresis with emphasis on its size dependence for separation. Then, we review theoretical and experimental aspects of diffusiophoretic separation in flows in both cross- and counter-gradient settings. This review aims to provide fundamental understanding and latest utilization of diffusiophoretic separation and further possible developments.

## II. DIFFUSIOPHORESIS

The physical origin of diffusiophoresis is the non-equilibrium solute-surface interactions. While electrostatics is the most commonly observed interaction, neutral solutes/colloids can also exhibit diffusiophoresis by other means such as dipole-dipole, van der Waals, and steric interactions.<sup>27</sup> Such interactions at out of equilibrium cause a pressure imbalance within the interaction layer, leading to tangential fluid flow. This interfacial flow simultaneously drives freely suspended particles to move in the opposite direction, a process known as phoretic migration.<sup>27</sup> As almost every recent paper on diffusiophoresis concerns electrostatic interactions, this review focuses mainly on long-range electrostatic interactions.

Concentration gradients of electrolytes can drive particle migration by two means. Ions with asymmetric diffusivities can induce spontaneous electric potential upon diffusion (Fig. 1, left panel). For symmetric electrolytes, the potential drop (often referred to as diffusion potential or liquid junction potential) is given as 43

$$\Delta \phi = -\beta \frac{k_B T}{ze} \int \nabla \ln c \cdot d\mathbf{x}, \tag{1}$$

where  $k_B$  is the Boltzmann constant, T is the temperature, z is the valence, and e is the elementary charge.  $\beta = (D_+ - D_-)/(D_+ + D_-)$ is the dimensionless diffusivity contrast, where  $D_{\pm}$  is the diffusivity of cation (+) and anion (-). This spontaneous electric potential difference can drive particle electrophoresis,

$$\boldsymbol{u}_{e} = f(\lambda) \cdot \frac{\epsilon \zeta \beta}{\eta} \frac{k_{B} T}{z e} \nabla \ln c, \qquad (2)$$

where  $\epsilon$  is the solution permittivity,  $\eta$  is the solution viscosity,  $\zeta$  is the particle zeta potential, and  $f(\lambda)$  is the size-dependent function that depends on  $\lambda = (\kappa a)^{-1}$ , which is the ratio of the Debye layer thickness  $\kappa^{-1}$  and the particle radius a. For an infinitesimally thin Debye layer where  $\lambda \to 0$ ,  $f(\lambda)$  reduces to unity, yielding the Smoluchowski equation.

In addition to the spontaneous electrophoresis, the electrostatic solute-surface interactions yield excess osmotic pressure within the interaction layer due to the attraction of counterions (Fig. 1, right panel). The local solute gradients can thus induce interfacial fluid flow by the osmotic pressure gradient that subsequently leads to particle motion, a process commonly known as chemiphoresis. The chemiphoretic velocity is given as

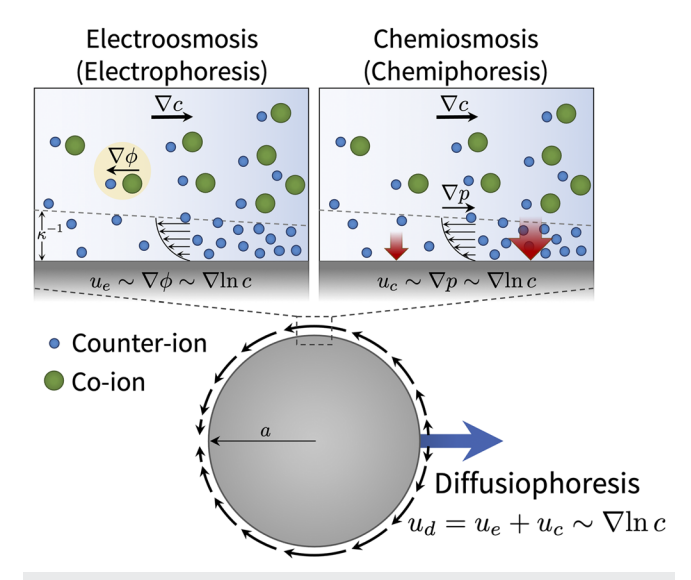


FIG. 1. Diffusiophoresis of a charged particle in a concentration gradient of a binary electrolyte. An ion pair within the yellow circle implies local electroneutrality, which is associated with a diffusion potential gradient  $abla \phi$ . The electric field caused by the buildup of diffusion potential induces electroosmotic flow within the Debye layer. Simultaneously, the osmotic pressure imbalance within the Debye layer drives (chemi)osmotic flow. As osmosis and phoresis are complementary phenomena, electroosmosis and chemiosmosis cause the particle to move in the opposite direction, a process known as diffusiophoresis

$$u_c = g(\lambda) \cdot \frac{4\epsilon}{n} \left(\frac{k_B T}{ze}\right)^2 \ln \left[\cosh\left(\frac{ze\zeta}{4k_B T}\right)\right] \nabla \ln c,$$
 (3)

where  $g(\lambda)$  is the size-dependent function for chemiphoresis, which also becomes unity when  $\lambda \to 0$ . The diffusiophoretic velocity is thus the linear combination of electrophoresis and chemiphoresis,

$$\mathbf{u}_d = \mathbf{u}_e + \mathbf{u}_c = \mathcal{M}_d(\lambda) \nabla \ln c,$$
 (4)

where  $\mathcal{M}_d(\lambda)$  is the size-dependent diffusiophoretic mobility that characterizes the tendency of a particle to migrate in response to local solute gradients by both electrophoresis and chemiphoresis. Generalized expressions for  $\mathcal{M}_d$  at infinitesimally thin Debye layer in asymmetric, multi-species electrolytes can be found in Refs. 44 and 45. It should be noted that in the event of solute gradients being highly non-linear at the scale of a particle size, then such a linear superposition of the two effects becomes invalid since Eqs. (2) and (3) are obtained by linearizing the solute gradients about a particle of interest.

What makes diffusiophoresis unique compared to conventional electrophoresis (i.e., electric field imposed by external power supply) is the extra contribution from chemiphoresis. Chemiphoresis, which always drives particles up the solute gradients under attractive solute-particle interactions, is not necessarily in the same direction as electrophoresis since the direction of electrophoresis depends on the sign of  $\zeta\beta$  [see Eq. (2)]. This non-linear feature also makes the size dependence non-monotonic due to the distinct size-dependent functions for electrophoresis  $f(\lambda)$  and chemiphoresis  $g(\lambda)$ . For example, when electrophoresis and chemiphoresis are in the opposite direction, smaller particles may actually exhibit stronger

diffusiophoresis contrary to common expectations in phoretic transport where the curvature suppresses the particle motion. Such unique features in diffusiophoresis enable a wide range of separation parameters—e.g., size, shape, and surface charge.

Prieve *et al.* first developed an analytical solution for the size-dependent diffusiophoresis in the limit of thin Debye layer ( $\lambda \ll 1$ ) using matched asymptotic expansion. <sup>13</sup> The expressions for  $f(\lambda)$  and  $g(\lambda)$  accurate to  $\mathcal{O}(\lambda)$  are given as

$$f(\lambda) = \left\{ 1 - \frac{\lambda k_B T}{2ze\zeta} \left[ F_1 + \frac{\epsilon}{2\eta D_s} \left( \frac{k_B T}{ze} \right)^2 (\beta F_4 + F_5) \right] \right\}^{-1}$$
 (5)

and

$$g(\lambda) = \left\{1 - \frac{\lambda}{8\ln\left[\cosh\left(\frac{ze\zeta}{4k_BT}\right)\right]} \cdot \left[F_0 + \frac{\epsilon}{2\eta D_s} \left(\frac{k_BT}{ze}\right)^2 (F_2 + \beta F_3)\right]\right\}^{-1},$$

where  $F_n$  are functions of the particle zeta potential. The full lengthy expressions are given in the Appendix of Ref. 13. Numerical values of  $F_n$  for a range of  $\zeta$  are also provided in Table 2 of Ref. 13 for convenient estimation of Eqs. (5) and (6).

Later, Keh and Wei studied size-dependent diffusiophoresis for arbitrary  $\lambda$ , but at small  $\zeta$ , i.e.,  $|\zeta| < k_B T/(ze)$  such that  $\ln[\cosh(ze\zeta/(4k_BT))] \approx 1/32(ze\zeta/(k_BT))^2$ . Using the regular perturbation method with  $\zeta$  as the perturbation parameter, the expression for the size-dependent functions  $f(\lambda)$  and  $g(\lambda)$  accurate to  $\mathcal{O}(\zeta^2)$  are given as

$$f(\lambda) = 1 - e^{\lambda^{-1}} \left[ 5E_7(\lambda) - 2E_5(\lambda) \right] \tag{7}$$

and

$$g(\lambda) = 1 + 4e^{\lambda^{-1}} \left[ E_3(\lambda) + 3E_4(\lambda) - \frac{7}{3}E_5(\lambda) - 5E_6(\lambda) \right]$$

$$+ e^{2\lambda^{-1}} \left[ \frac{10}{3}E_6(2\lambda) - 40E_3(\lambda)E_7(\lambda) - 40E_5(\lambda)E_7(\lambda) + \frac{7}{3}E_8(2\lambda) \right],$$
 (8)

where  $E_n(\lambda) = \int_1^\infty t^{-n} e^{-t/\lambda} dt$ . For convenience, Eqs. (7) and (8) may be expressed using the curve fits as  $f(\lambda) = 1 - 0.33/(1 + 0.072\lambda^{-1.1})$  and  $g(\lambda) = 1 - 1/(1 + 0.085\lambda^{-1.1} + 0.020\lambda^{-0.1})$ , which can cover any positive  $\lambda$  value with good accuracy. <sup>46,47</sup>

As an example, the size-dependent diffusiophoretic mobility  $\mathcal{M}_d(\lambda)$  of charged colloids immersed in NaCl is given in Fig. 2. Figure 2(a) is the mobility obtained by Prieve *et al.* [Eqs. (5) and (6)], <sup>13</sup> and Fig. 2(b) is that obtained by Keh and Hsu [Eqs. (7) and (8)]. <sup>46</sup> As expected, both models show good agreement to each other only at small  $\zeta$  and  $\lambda$  values (cf. solid curves at  $\lambda \ll 1$ ). In light of the proper usage of these two models, Prieve's model would be more suitable for highly charged, large particles in concentrated solutions (i.e., large  $\zeta$  and small  $\lambda$ ), whereas Keh's model is more suitable for moderately charged nanoparticles in dilute solutions (i.e., small  $\zeta$  and large  $\lambda$ ).

Another peculiar feature that arises due to chemiphoresis is the non-zero surface force. 48 A particle undergoing pure electrophoresis is known to exhibit zero net force within the Debye layer as the hydrodynamic stress caused by electroosmosis and the electrostatic force acting on the particle surface charge are precisely balanced. 49

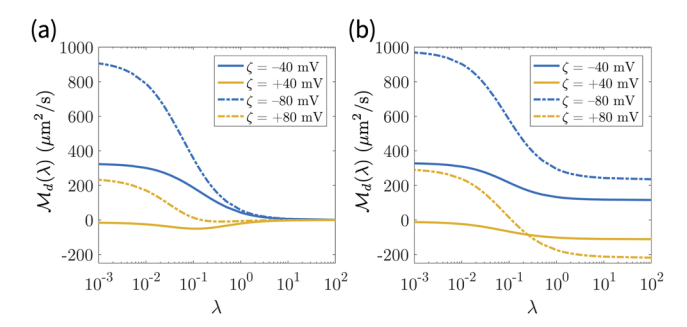


**FIG. 2.** Size-dependent particle diffusiophoretic mobility  $\mathcal{M}_d(\lambda)$  for various particle zeta potentials. The solute is NaCl. (a) Prieve's model [Eqs. (5) and (6)]. (b) Keh's model [Eqs. (7) and (8)]. (4)

In contrast, a particle undergoing diffusiophoresis (chemiphoresis) does not show such a net zero surface force due to the presence of the excess osmotic pressure gradient. A full analytical derivation of the local force balance on a diffusiophoretic particle can be found in the recent work by Marbach *et al.* Such a non-vanishing surface force that varies along the particle surface upon diffusiophoresis can lead to appreciable deformation of soft colloids such as drops, vesicles, and polymers, suggesting particle separation based on deformability. Such as drops are deformability.

# III. CROSS-GRADIENT DIFFUSIOPHORESIS

## A. Theory

The cross-gradient diffusiophoresis involves particle diffusiophoresis acting perpendicular to the flow by the transverse solute diffusion (Fig. 3). The idea of using transverse diffusion for continuous separation dates back decades ago. One representative example is the microfluidic H-filter (or T-sensor), which relies on the Brownian diffusion of particles for enabling size-dependent colloid separation. Diffusiophoresis differs from the H-filter by the fact that the diffusiophoresis relies on the diffusion of molecular solutes to enhance the motion of larger colloidal particles, typically orders of magnitude faster than their Brownian counterpart.

Transverse gradients in channel flows can be established in a number of ways such as co-flowing multiple solutions in parallel, <sup>8,52</sup> imposing reacting walls, <sup>53–55</sup> or flowing reactive colloids that can generate or consume solutes. <sup>56</sup> The solute distribution is governed by the fluid flow, diffusion, and reaction, which determines the particle diffusiophoresis. Conservation equations for mass, momentum, solutes (electrolytes), and particles are given as

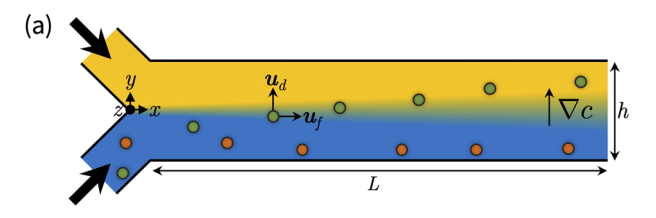
$$\nabla \cdot \boldsymbol{u}_f = 0, \tag{9}$$

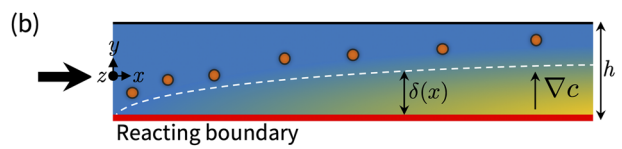
$$\rho \frac{\partial \boldsymbol{u}_f}{\partial t} + \rho \boldsymbol{u}_f \cdot \nabla \boldsymbol{u}_f = -\nabla p + \eta \nabla^2 \boldsymbol{u}_f, \tag{10}$$

$$\frac{\partial c_i}{\partial t} + \nabla \cdot \left( c_i \boldsymbol{u}_f - \frac{z_i D_i}{k_B T} c_i \nabla \phi \right) = D_i \nabla^2 c_i + r_i, \tag{11}$$

and

$$\frac{\partial n}{\partial t} + \nabla \cdot (n\mathbf{u}_f + n\mathbf{u}_d) = D_p \nabla^2 n, \tag{12}$$





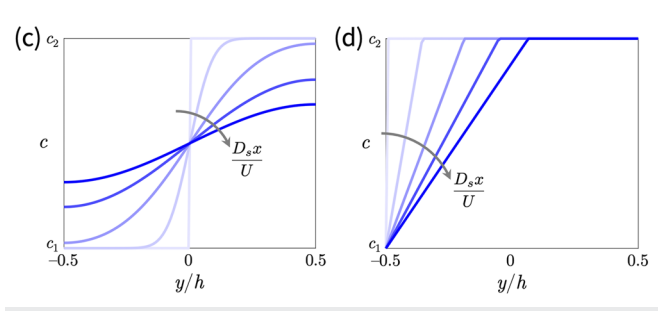


**FIG. 3**. Continuous diffusiophoretic separation in cross-gradient settings. The solute gradients transverse to the flow can be established by (a) co-flowing multiple solutions or (b) placing reactive walls. [(c) and (d)] Approximated solute profile evolution along downstream (x direction) in (c) co-flow [Eq. (16)] and (d) reactive wall settings [Eq. (17)].

where  $u_f$  is the fluid velocity, p is the fluid pressure,  $\rho$  is the fluid density,  $\eta$  is the fluid dynamic viscosity,  $c_i$  is the solute concentration of ith species,  $D_i$  is the diffusivity of ith solute species,  $r_i$  is the rate of homogeneous reaction of ith species, n is the particle concentration,  $D_p$  is the particle diffusivity, and  $u_d$  is the particle diffusiophoretic velocity. Equation (11) is the Nernst–Planck equation that can be reduced to a single species advection–diffusion–reaction equation for binary electrolytes satisfying local electroneutrality ( $c_+ = c_- = c_i$ ),

$$\frac{\partial c}{\partial t} + \nabla \cdot (c\mathbf{u}_f) = D_s \nabla^2 c + r, \tag{13}$$

where  $D_s = 2D_+D_-/(D_+ + D_-)$  is the ambipolar solute diffusivity.

For shallow microfluidic channels where the width h is much larger than the depth d of the channel, i.e.,  $h/d \gg 1$ , the flow profile can be approximated as a Hele–Shaw flow as  $u_f \approx u_x(z)\hat{\mathbf{i}} = 3U/2 \cdot (1-4z^2/d^2)\hat{\mathbf{i}}$ , where U is the depth-averaged flow velocity. This approximation is only valid away from the side walls (|y| < h/2 - d). Neglecting reaction and assuming steady state, Eq. (13) can be reduced to the following solute boundary layer equation:

$$u_x(z)\frac{\partial c}{\partial x} = D_s \left(\frac{\partial^2 c}{\partial y^2} + \frac{\partial^2 c}{\partial z^2}\right). \tag{14}$$

The solute diffusion in the x direction has been neglected as the advection dominates over diffusion in the streamwise direction in most microfluidics applications.<sup>57</sup> Furthermore, for sufficient distance downstream over which the solute has diffused across the channel depth (e.g.,  $x > 0.03Ud^2/D_s^{57}$ ), the solute concentration

becomes independent of z. Thus, Eq. (14) reduces to the following equation:

$$U\frac{\partial c}{\partial x} = D_s \frac{\partial^2 c}{\partial v^2}.$$
 (15)

For two streams co-flowing in parallel where the concentration of one stream is  $c_1$  and that of the other is  $c_2$  [Fig. 3(a)] such that the inlet condition is  $c(x = 0, y) = c_1 + (c_2 - c_1)H(y)$ , where  $H(\cdot)$  is the heaviside step function, and the boundary conditions are no-flux conditions on the walls, then the solution to Eq. (15) can be obtained using the method of images as

$$c(x,y) = c_1 + \frac{(c_2 - c_1)}{2} \sum_{k=-\infty}^{\infty} \left[ \operatorname{erf}\left(\frac{y + 2kh}{\sqrt{D_s x/U}}\right) - \operatorname{erf}\left(\frac{y - h + 2kh}{\sqrt{D_s x/U}}\right) \right],$$
(16)

which is presented in Fig. 3(c). This solution is also applicable to symmetric co-flow (flow-focusing) settings in which the concentration of the outer sheath streams differs from the inner stream by taking symmetry about  $y = \pm h/2$ .

Another way of creating chemical gradients is to introduce chemical reactions. In this case, the transverse solute gradients can be achieved by having a reactive sidewall [Fig. 3(b)]. Examples include feeding soluble gases through a permeable wall<sup>53,54</sup> or placing ion exchange media at the wall. 55 To obtain the complete solute profile in the presence of reaction, it is required to solve a set of coupled Nernst-Planck equations for every ionic species. However, if the dominant species participating in diffusiophoresis is binary (e.g., Ref. 53) and implicitly assuming local electroneutrality, then we can use the regular diffusion-advection-reaction equation for describing the solute profile [Eq. (13)]. Moreover, a homogeneous reaction term can be simplified to a heterogeneous surface reaction with a constant boundary condition if the reaction occurs in the vicinity of the wall and is fast such that the surface Damköhler number is high (i.e.,  $Da_s = k_s h/D_s \gg 1$ , where  $k_s$  is the surface reaction rate constant).

For such cases, the gradients of reacting species are established near the wall so that a boundary layer analysis can be performed to approximate the solute profile. For channels where the parabolic flow profile in the transverse direction (*y*-direction) within the boundary layer is valid (e.g., flow near a side wall in shallow rectangular channels, 2D slit flow, or pipe flow), an approximate solution for the boundary layer can be obtained. Adapting the work of Lee *et al.* for a 2D slit flow  $[u_x(y) = 3U/2 \cdot (1 - 4y^2/h^2)]$ , <sup>55</sup> the solute profile may be treated as linear within the boundary layer. This approximation gives the following expression for the solute profile [Fig. 3(d)]:

$$c(x,y) = \left[1 - H(y - \delta)\right] \left[\frac{2(c_2 - c_1)(y - \delta)}{h + 2\delta}\right] + c_2, \quad (17)$$

where  $c_2$  is the background ion concentration and  $c_1$  is the concentration created at the reactive boundary. Here,  $\delta(x) \approx (3D_shx/(4U))^{1/3}$  is the boundary layer thickness obtained by integrating Eq. (15) across the boundary layer provided  $\delta \ll h$ . The 1/3 scaling is in accordance with solute dispersion in flows near boundaries in rectangular channels.  $^{57,58}$ 

Particles can migrate from the established solute gradients in the transverse direction (*y*-direction) by diffusiophoresis.

The solute profiles obtained by solving Eq. (13) [e.g., Eqs. (16) and (17)] are used to solve for the transverse diffusiophoresis using Eq. (4),  $\mathbf{u}_d = \mathcal{M}_d \partial_y \ln c \hat{\mathbf{j}}$ , which determines the particle dynamics. For instance, one can immediately derive the non-Brownian particle trajectory by integrating the equation of motion  $dy/dx = u_d/U$ . The particle density profile can be obtained by solving the particle advection–diffusion equation [Eq. (12)], which is typically performed numerically.

The separation performance depends on two characteristic time scales, the advection (residence) time in the streamwise direction ( $t_f \sim L/U$ , where L is the channel length) and the diffusiophoresis time in the transverse direction ( $t_d \sim h^2/\mathcal{M}_d$ ). Comparing these two time scales leads to the definition of a particle Péclet number,  $\text{Pe}_p = Uh^2/(L\mathcal{M}_d)$ , which provides the basis for the design of separation processes in cross-gradient settings.

# **B.** Experiments

# 1. Cross gradients by co-flowing

A number of recent studies have demonstrated the implementation of diffusiophoresis for colloid separation in cross-gradient settings by co-flowing multiple solutions. While there have been several reports on diffusiophoresis indicating its utility in separation dating back to the 1980s, <sup>14,59</sup> the first study on the use of diffusiophoresis in continuous microfluidics separation was reported by Abécassis *et al.* decades later in 2008. <sup>8,60</sup> They used a symmetric coflow device in which the inner colloidal stream is surrounded by the outer buffer streams [Fig. 4(a)]. This configuration allows the transverse gradient and the subsequent colloid diffusiophoresis to occur symmetric about the centerline, where the transverse solute profile can be expressed using Eq. (16) given above.

The colloid dispersion along the downstream is shown in Fig. 4(b), which depends on the imposed solute gradients. For small x where the solute profile reduces to a single term from the series solution in Eq. (16), the colloid dispersion width w(x) is found by integrating  $dy/dx = u_d/U$  at the interface of the two solutions  $[y(x = 0) = w_0/2]$ , where  $w_0$  is the initial colloid width]. The colloid width along the downstream is given as

$$w(x) = w_0 \pm \sqrt{\frac{16}{\pi}} \left[ \frac{D_s}{\mathcal{M}_d} \left( 1 + \frac{2c_2}{c_1} \right) + \frac{2}{\pi (1 + 2c_2/c_1)} \right]^{-1} \sqrt{\frac{D_s x}{U}},$$
(13)

where the sign depends on the direction of diffusiophoresis {e.g., (+) for outward spreading [center panel in Fig. 4(b)] and (-) for inward focusing [right panel in Fig. 4(b)]}. As expected, the colloid width shows diffusive dispersion in which w(x) scales as  $w(x) \sim (x/U)^{1/2}$  [Fig. 4(c)]. Far downstream where the solutes have fully diffused laterally across the channel [i.e.,  $y \approx U(h/2)^2/2D_s$ ], the terminal colloid width neglecting particle diffusion is found as

$$w_{\infty} \approx w_0 \sqrt{\frac{8}{\pi}} \left[ \frac{D_s}{\mathcal{M}_d} (1 + 2c_2/c_1) + \frac{2}{\pi (1 + 2c_2/c_1)} \right]^{-1},$$
 (19)

which is determined by the solute contrast  $(c_2/c_1)$  and the particle and solute pair  $(\mathcal{M}_d/D_s)$ . Equation (19) shows a good agreement with experimental observations from various solutes [Fig. 4(d)], which could serve as a useful guideline for designing split outlets in co-flow separation systems.

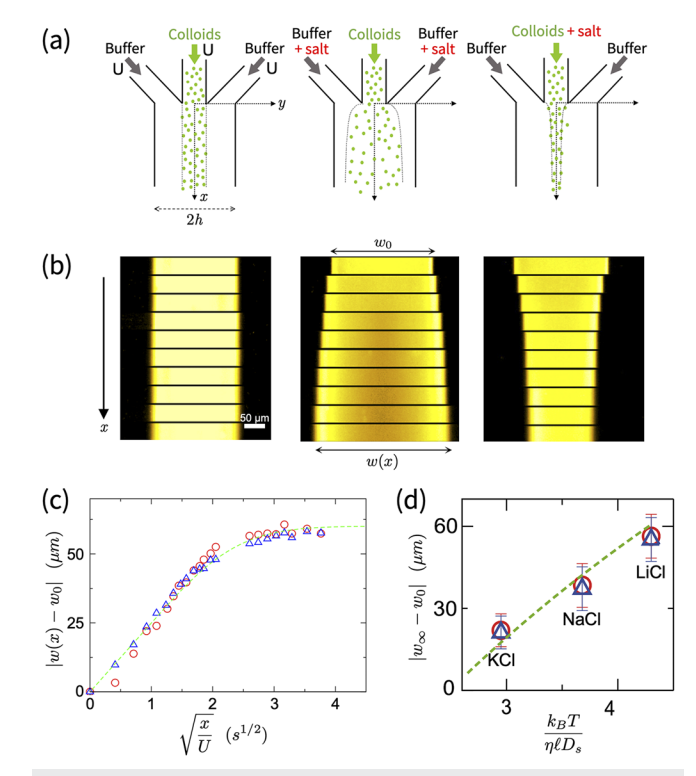


**FIG. 4.** Cross-gradient diffusiophoresis in co-flow settings. <sup>8,60</sup> (a) Particle stream is fed through the inner stream and the buffer solutions are fed through the outer streams. Either stream may contain additional solutes so that the transverse solute gradients can be established. (b) Fluorescence imaging of particles [polystyrene latex (PS), particle radius  $a=0.1~\mu\text{m}$ ] along downstream for various solute configurations (left panel—no solute contrast, center panel—outer streams contain 10 mM LiCl, and right panel—inner stream contains 10 mM LiCl). w(x) is the width of the colloid band. (c) Change in colloid width along the downstream direction. Dashed line is Eq. (18). (d) The terminal colloid width for various solutes. Here,  $\ell=(ze)^2/(4\pi\epsilon k_BT)=0.7$  nm is the Bjerrum length of water at room temperature. Dashed line is Eq. (19). Reproduced with permission from Abécassis *et al.*, "Osmotic manipulation of particles for microfluidic applications," New J. Phys. 11, 075022 (2009). Copyright 2009 Author(s), licensed under a Creative Commons Attribution 3.0 Unported License.

In a similar symmetric co-flow setting, Visan and Lammertink recently demonstrated that a transverse colloid diffusiophoresis can be enabled by introducing reactive particles [Fig. 5(a)]. When photocatalytic particles (TiO<sub>2</sub>) are injected through the middle stream, the particles react with the solution upon UV illumination, creating (or consuming) chemical species uniformly around the particles. Having particles only in the inner stream, transverse solute gradients are subsequently created along which the particles can migrate via diffusiophoresis. This is seemingly identical to light-activated self-diffusiophoretic particles (e.g., SiO<sub>2</sub>-Fe<sub>2</sub>O<sub>3</sub> Janus particles<sup>61</sup>). However, the key difference is that unlike the self-diffusiophoretic particles where an individual particle creates solute gradients localized to the scale of its own body length, thereby moving on its own (hence commonly referred to as "active matter"), here, the solute gradients are created by the asymmetric particle distribution, thus requiring multiple particles to break symmetry.62

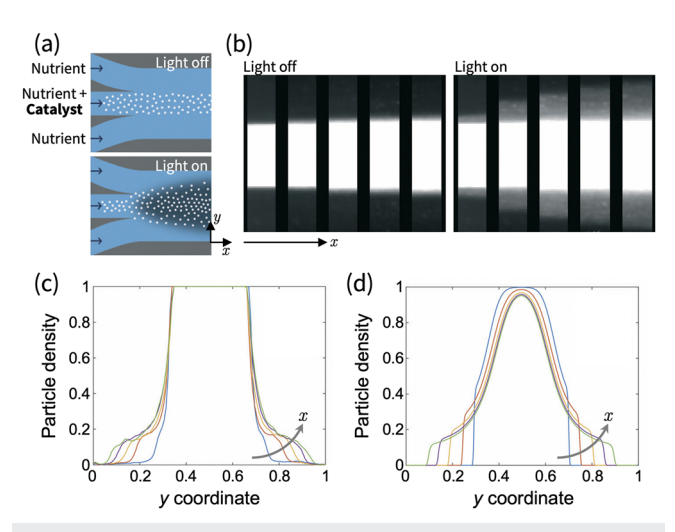


**FIG. 5**. Cross-gradient diffusiophoresis enabled by photoreacting particles.  $^{56}$  (a) Nutrients (methylthioninium chloride) are added to all three streams, while photocatalytic particles (TiO2,  $a=80\,\mathrm{nm}$ ) are only present in the inner stream. Such an uneven particle distribution creates transverse nutrient gradients during photocatalytic degradation, leading to diffusiophoresis of TiO2 particles. (b) Particle distribution at different positions in the downstream direction. The numbers correspond to the residence time (left panel—without photoreaction and right panel—with photoreaction). (c) Transverse particle profile obtained from the fluorescence intensity in the right panel of (b). (d) Numerically modeled transverse particle density profile. Reproduced with permission from A. Visan and R. G. Lammertink, "Reaction induced diffusiophoresis of ordinary catalytic particles," React. Chem. Eng. **4**, 1439–1446 (2019). Copyright 2019 Author(s), licensed under a Creative Commons Attribution 3.0 Unported License.

In the absence of photoreaction, the particles disperse laterally only by diffusion [Fig. 5(b), left panel]. Illuminating UV light on the particle stream triggers photodissociation of the solutes (methylthioninium chloride), which lowers the solute concentration in the middle stream containing particles. This transverse solute gradient eventually leads to transverse diffusiophoresis, as shown in Figs. 5(b) (right panel) and 5(c). By treating the catalytic particles as a homogeneous point sink, the coupled solute–particle distribution can be modeled numerically by solving Eqs. (12) and (13), where the reaction term is a function of both the solute and the particle concentration. The photoreaction is assumed to be a first-order homogeneous reaction r = -kc, where k is the reaction rate constant that is proportional to the particle concentration such that  $r \sim nc$ . The simulation results well capture the reaction-induced particle migration, as shown in Figs. 5(c) and 5(d).

Diffusiophoresis does not necessarily have to operate as a stand-alone mechanism for particle migration. Combination of other processes such as external electrophoresis may provide synergistic separation performance. A recent study by Lee *et al.* demonstrated that the simultaneous use of a small external electric field may allow enhanced, non-linear cross-gradient diffusiophoresis. <sup>52</sup> The authors fabricated a co-flow device in which the transverse solute gradients are established by leaky walls made of self-assembled latex particles and imposed simultaneous solute and external electric potential gradients transverse to the flow [Fig. 6(a)]. The leaky walls serve as a means to allow only diffusion of solutes across the

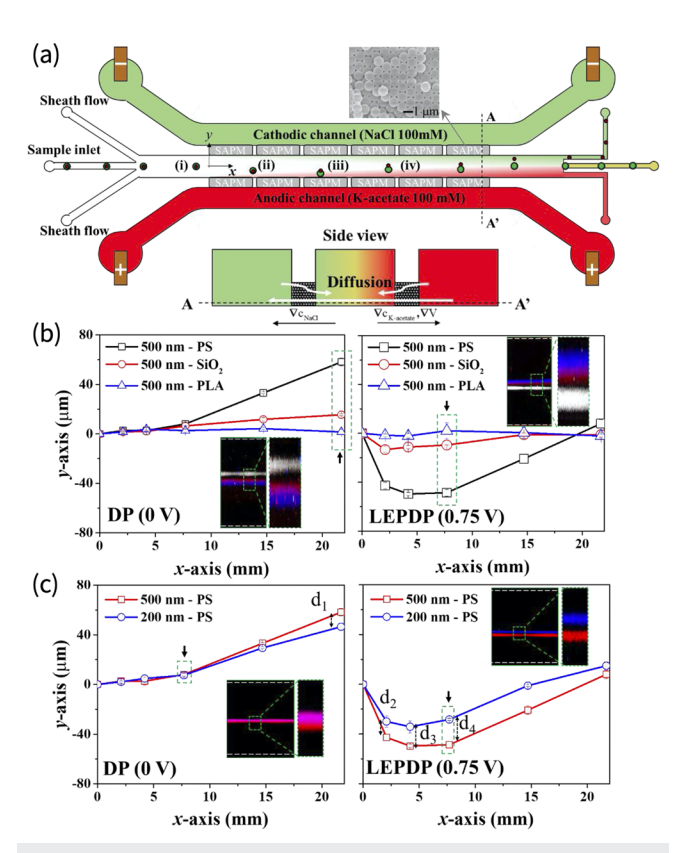


FIG. 6. Cross-gradient particle separation enhanced by the combination of diffusiophoresis and low-potential electrophoresis [low-electric-potential-diffusiophoresis (LEPDP)].<sup>52</sup> (a) Experimental setup. The middle channel is filled with particle suspension and the two side channels are filled with 100 mM NaCl (upper) and potassium acetate (KAc) solution (lower). The flow channels are loosely separated by porous membranes [self-assembled particle membranes (SAPM)], which enables transverse gradients. A scanning electron microscope image of SAPM is shown in the upper panel. Electrodes are immersed in the side channels to drive LEPDP. Cross section of A-A' is shown in the lower panel. (b) Trajectories of particles with varying zeta potential [PS, silica (SiO<sub>2</sub>), and polylactide (PLA)], but having same size ( $a = 0.25 \mu m$ ), either by only diffusiophoresis (left panel) or by LEPDP (right panel). The maximum transverse separation occurs more upstream (green boxes) when a small potential drop (0.75 V) is supplemented externally. (c) Similar to (b) but with particles having the same zeta potential (PS) with different sizes ( $a = 0.25 \mu m$  and 0.1  $\mu m$ ). Reproduced with permission from Lee et al., "Low-electric-potential-assisted diffusiophoresis for continuous separation of nanoparticles on a chip," Lab Chip 20, 2735-2747 (2020). Copyright 2020 Royal Society of Chemistry.

streams while preventing transverse advection, which is analogous to hydrogel barriers used in linear gradient devices. <sup>21,63–65</sup>

While the transverse solute gradients in the particle stream are developed gradually along downstream, the electric field is established immediately across the entire channel. However, this external electric field weakens downstream due to the gradual increase in the electrical conductivity of the middle stream by the addition of solutes. Consequently, the particle electrophoresis begins immediately upstream and gradually weakens downstream, whereas diffusiophoresis develops gradually downstream. The combination of

two effects arising in different downstream locations makes the particle transverse trajectory non-monotonic [Figs. 6(b) and 6(c)]. This strategy can be used to reduce the separation distance for efficient, miniaturized separation [Fig. 6(b)] or enable particle separation that is otherwise unable to achieve by diffusiophoresis alone [Fig. 6(c)].

## 2. Cross gradients by wall reaction

Alternatively, transverse solute gradients can be created by introducing heterogeneous surface reactions from channel walls. Examples include the use of soluble gases<sup>53,54</sup> or ion exchange media.<sup>55</sup> Shin *et al.* demonstrated that  $CO_2$  can be utilized to induce diffusiophoresis for continuous colloid separation.  $CO_2$  can be a favorable diffusiophoresis agent as the dissociated ion pair  $(H^+/HCO_3^-)$  has a large  $\beta$  such that it may induce strong electrophoresis. With a microfluidic device made out of polydimethylsiloxane (PDMS), which has excellent  $CO_2$  permeability, <sup>66</sup>  $CO_2$  gas can be fed through a side channel placed in the vicinity of the particle stream [Fig. 7(a)]. The permeated  $CO_2$  gas dissolves and subsequently dissociates into ions in the flow stream, enabling particle diffusiophoresis transverse to the flow [Fig. 7(b)]. An empty air

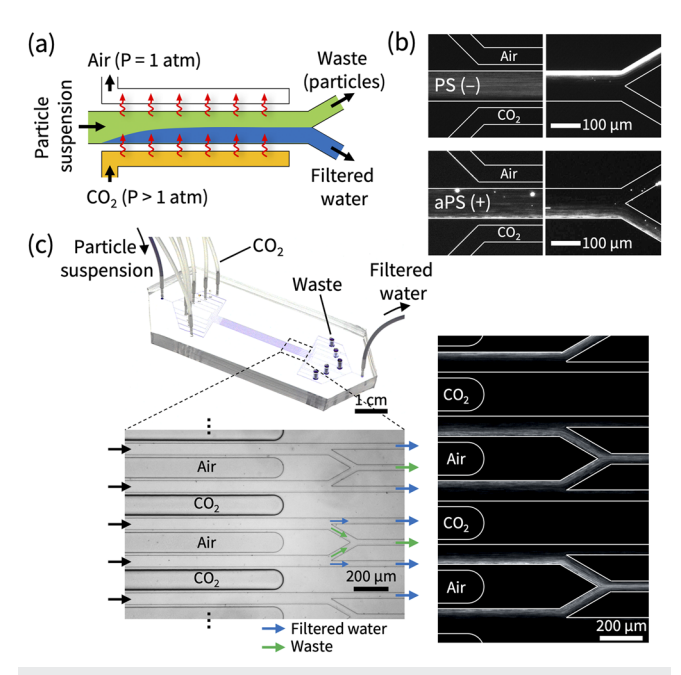


**FIG. 7.** Cross-gradient diffusiophoresis by CO<sub>2</sub> dissolution. <sup>53</sup> (a) Experimental setup. The gas-permeable channel [polydimethylsiloxane (PDMS)] allows CO<sub>2</sub> gas to permeate and dissolve into the particle stream, inducing transverse diffusiophoresis. The air channel prevents saturation of CO<sub>2</sub> in the suspension, thus extending the transverse particle migration. (b) Fluorescence microscopy images of negatively charged (PS, a = 0.25  $\mu$ m; upper panels) and positively charged particles [amine-functionalized polystyrene (aPS), a = 0.5  $\mu$ m; lower panels] migrating transverse to the flow. Images are taken near the entrance (left panels) and exit (right panels) of the flow channel. (c) Upscaled separation device having ten parallel flow channels in a monolithic PDMS block. Right panel is the fluorescence image of PS particles near the exit. Reproduced with permission from Shin et al., "Membraneless water filtration using CO<sub>2</sub>," Nat. Commun. **8**, 15181 (2017). Copyright 2017 Author(s), licensed under a Creative Commons Attribution 4.0 license

channel is placed on the other side of the stream to prevent saturation of  $CO_2$  in the particle stream, which helps to sustain concentration gradients and enable long-lasting diffusiophoresis.

Due to the scalability of the device design, the authors demonstrated an upscaled device by placing  $CO_2$  and air channels alternatively, thus achieving higher throughput [Fig. 7(c)]. Another benefit of using  $CO_2$  for separation is its ability to self-equilibrate with the atmosphere. Any excess  $CO_2$  can be removed spontaneously without the need for post removal and can be reused for multiple rounds for improved separation efficacy.

The use of CO<sub>2</sub> for continuous separation was further applied to separate hard-to-separate colloids such as nanoparticles and nanoemulsion.<sup>54</sup> As the dissociated ion pair gives opposite electrophoresis and chemiphoresis for negatively charged particles, this offers a non-linear particle control over its size as mentioned earlier in Sec. II. For instance, the size dependence in CO<sub>2</sub> diffusiophoresis shows that the finite size effect enhances diffusiophoresis for negatively charged nanoparticles [Fig. 8(a)], thus adding an extra degree of freedom to control the nanoparticle position and, ultimately, the particle composition of the outlet streams [Fig. 8(b)].

Moreover, given that highly charged particles experience significant diffusiophoresis, particles with a low surface charge can also be manipulated with the aid of more highly charged particles as a "vehicle" provided that the separating colloids can adhere to the highly charged particles. Using this concept, Shimokusu *et al.* recently demonstrated the separation of decane nanoemulsion. <sup>54</sup> Once the decane drops are adhered to the highly charged particles [carboxylate-functionalized polystyrene; Fig. 8(c)], the particles can

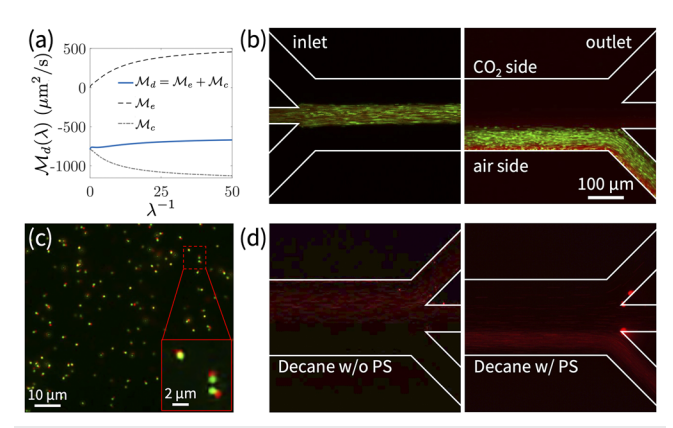


**FIG. 8.** Separation of nanoparticles and nanoemulsion by  $\mathrm{CO}_2$ -enabled diffusiophoresis. [(a) and (b)] Separation of nanoparticles by size-dependent diffusiophoresis. (a) Electrophoretic mobility ( $\mathcal{M}_e$ , dashed curve) and chemiphoretic mobility ( $\mathcal{M}_e$ , dashed-dotted curve) being opposite for negatively charged particles in  $\mathrm{CO}_2$  gradients results in the enhancement of diffusiophoretic mobility ( $\mathcal{M}_d = \mathcal{M}_e + \mathcal{M}_e$ , blue curve) by the size effect (i.e.,  $\mathcal{M}_d$  increases with  $\lambda$ ). (b) This enables nanoparticles (PS, a=30 nm, red fluorescence) to migrate stronger than microparticles (cPS,  $a=0.5~\mu\mathrm{m}$ , green fluorescence). [(c) and (d)] Separation of decane nanoemulsion by the use of diffusiophoresis of "vehicle" particles. (c) Fluorescence image of cPS-decane mixture. Green indicates cPS and red indicates decane drops. The inset is a close-up image showing aggregated cPS-decane pairs. (d) Fluorescence images of decane drops with (right panel) or without (left panel) cPS vehicle particles. Reproduced with permission from Shimokusu *et al.*, "Colloid separation by  $\mathrm{CO}_2$ -induced diffusiophoresis," Langmuir **36**, 7032–7038 (2020). Copyright 2020 American Chemical Society.

be used as vehicles to facilitate the transverse migration of oil drops, which would otherwise not experience significant diffusiophoresis [Fig. 8(d)]. This approach may be potentially utilized in the separation of neutrally charged, hydrophobic biocolloids such as proteins or drug nanoparticles<sup>67</sup> or post processing in oil extraction or wastewater treatment where emulsified oil drops are relatively insensitive to conventional separation techniques, such as sedimentation and centrifugation.<sup>68</sup>

Heterogeneous chemical reactions can also be achieved in continuous flow settings using commercially available ion exchange materials such as Nafion, Fumacep, Neosepta, and Selemion.<sup>69</sup> First shown by Florea *et al.* is that colloidal particles around Nafion membrane can experience substantial diffusiophoresis due to the solute gradients established by the cation exchange,<sup>70</sup> Lee *et al.* have implemented this material to achieve continuous separation in flow.<sup>55</sup> By placing two strips of Nafion in parallel, the authors created a microfluidic channel consisting of reactive side walls [Fig. 9(a)].

While the ion exchange process is inherently associated with multiple ionic species, such a process in Nafion can be reduced to

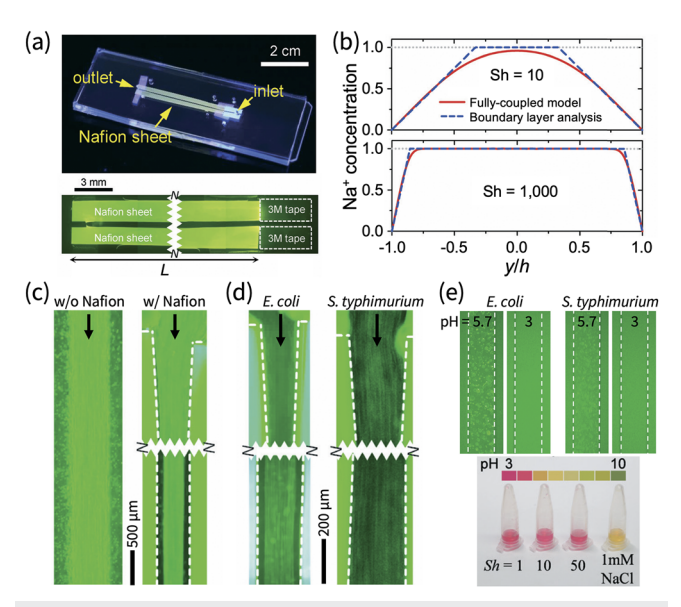


FIG. 9. Cross-gradient diffusiophoresis enabled by ion-exchanging walls.<sup>55</sup> (a) Experimental setup. A flow channel is created by placing two strips of ion exchange membranes (Nafion) in parallel. As the particle suspension flows along the channel, the ion exchange process creates a transverse gradient, thus enabling particle diffusiophoresis. (b) Approximate transverse solute profile obtained by singlespecies boundary layer analysis [blue dashed curves, Eq. (17)]. Red solid curves indicate numerical solution from the fully coupled, multi-species Nernst-Planck equation. Here, Sh is the Sherwood number defined as Sh =  $Uh^2/(LD_s)$ , analogous to the particle Péclet number defined in the main text. (c) Particles (PS,  $a = 0.5 \mu m$ ) with (right panel) or without (left panel) Nafion. (d) Bacteria separation by cross-gradient separation. E. coli (left panel) shows noticeable transverse migration, while S. typhimurium (right panel) shows no apparent difference. (e) Reduced bacteria activity at low pH. The bottom panel shows the pH of effluent, indicating low pH. Reproduced with permission from Lee et al., "Diffusiophoretic exclusion of colloidal particles for continuous water purification," Lab Chip 18, 1713-1724 (2018). Copyright 2018 Royal Society of Chemistry.

a two-species transport problem using local neutrality and water equilibrium (e.g., NaCl and HCl). This allows a simplified boundary layer analysis, as shown in Eq. (17), that agrees reasonably well with the solute profile obtained by solving a set of fully coupled Nernst–Planck equations numerically [Fig. 9(b)]. The gradients established in the solute boundary layer drive the transverse particle diffusiophoresis [Fig. 9(c)].

The authors used this device to separate suspended bacteria such as *Escherichia coli* and *Salmonella typhimurium*. While *E. coli* was able to separate via diffusiophoresis, *S. typhimurium* did not show any noticeable transverse migration due to its low surface charge [Fig. 9(d)]. Nevertheless, the authors confirmed that the Nafion-based device still managed to remove *S. typhimurium* due to the reduced pH enabled by the ion exchange process [Fig. 9(e)]. Such demonstrations show potential utility in portable water treatment for removing waterborne pathogens without the need of excess chemicals (e.g., chlorination) or energy-intense processes (e.g., UV treatment).

## IV. COUNTER-GRADIENT DIFFUSIOPHORESIS

### A. Theory

Counter-gradient diffusiophoresis involves two different streams merging at a junction in a way that the solute gradients are established counter to the flow. Such gradients can be created by merging two flow channels [Fig. 10(a)] or by connecting a flow channel to a stagnant reservoir [Fig. 10(b)]. The advantage of counter-flow configuration is that the fluid advection creates steep, steady-state gradients, leading to stronger diffusiophoresis contrary to systems governed mainly by diffusion, which are involved in a number of diffusiophoresis studies. <sup>59,70-78</sup> While the counter-gradient diffusiophoresis may naturally arise in flow networks and porous media, this phenomena can also be exploited for rapid bioassays due to its ability to locally concentrate biocolloids.

A typical situation is illustrated in Fig. 10(a). Consider a horizontal flow channel connected perpendicular to another flow channel containing different solution. The solute gradient is established within the horizontal channel due to the channel flow and solute diffusion. Suspended particles can experience an equilibrium position somewhere in the horizontal channel, which is when the sum of the diffusiophoresis force and the viscous drag acting on the particle is zero. The solute and particle dynamics in such settings are recently studied by Shin *et al.* <sup>79</sup> and Ault *et al.* <sup>80</sup> Assuming that the horizontal channel is long and narrow, and the solute concentration at the merging junction is held constant via the flow from the vertical channel, then the solute and particle dynamics in the horizontal channel can be approximated as a 1D problem. The steady-state solute profile can be found by solving a 1D steady-state advection—diffusion equation with constant boundary conditions, which is given as

$$c(x) = c_1 + (c_2 - c_1) \frac{e^{\frac{Ux}{D_s}} - 1}{e^{\frac{Uz}{D_s}} - 1},$$
(20)

where  $c_1$  is the concentration at x = 0,  $c_2$  is the concentration at x = L, and U is the average flow velocity inside the horizontal channel. The solute profile is set by the solute Péclet number  $Pe_s = UL/D_s$  [Fig. 10(c)].

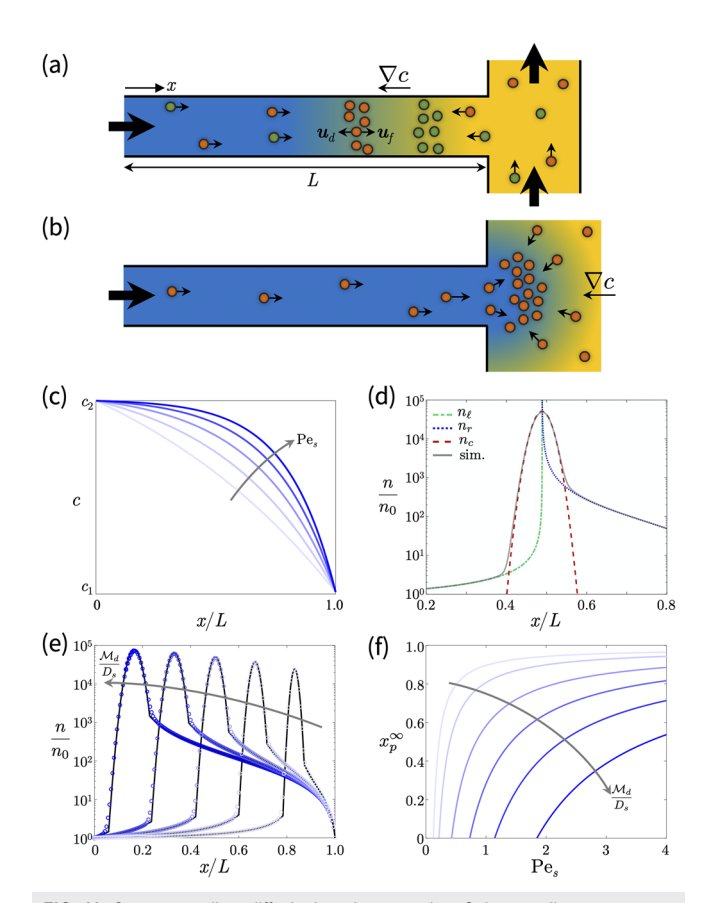


FIG. 10. Counter-gradient diffusiophoretic separation. Solute gradients counter to the fluid flow can be established by (a) merging two flow streams or (b) exiting a stream to a large reservoir containing a different solution. (c) Steady-state solute profile in the horizontal channel established by fluid advection and solute diffusion [Eq. (20)]. (d) Particle profile in the channel described by distinct dynamics in three different regions. To the left and right of the peak, particle dynamics is dominated by fluid advection and diffusiophoresis where the particle diffusion is negligible, and the particle distribution is well represented by steady-state solutions given in Eq. (21)  $(n_{\ell})$  and Eq. (22)  $(n_r)$ . Near the equilibrium position, the transient particle distribution is determined by the fluid advection, particle diffusiophoresis, and particle diffusion, denoted as  $n_c$  [Eq. (26)]. Numerical results (solid curve) are provided for comparison. (e) Particle density profiles for different particle mobilities. Solid curves represent analytical results from the piecewise solutions, whereas symbols represent numerical results. (f) Steady-state particle equilibrium location  $x_n^{\infty}$  as a function of the solute Péclet number Pes for a variety of particle mobilities. (d)-(f) are reproduced with permission from J. T. Ault, S. Shin, and H. A. Stone, "Diffusiophoresis in narrow channel flows," J. Fluid Mech. 854, 420-448 (2018). Copyright 2018 Cambridge University Press.

The dynamics of particles experiencing diffusiophoresis in the horizontal channel can be obtained by solving Eqs. (12) and (13) in 1D. Ault *et al.* performed matched asymptotic expansion to obtain piecewise solutions for the particle profile in this system. <sup>80</sup> Neglecting particle diffusion, the solutions for the particle density near the left (x = 0) and right ends (x = L) of the channel are given as

$$n_{\ell}(x) = F(x) \cdot n_0 \left[ 1 + \frac{\mathcal{M}_p}{D_s} \frac{(c_2 - c_1)}{c_1(e^{\frac{UL}{D_s}} - 1)} \right]$$
 (21)

and

$$n_r(x) = F(x) \cdot n_0 \left[ 1 + \frac{\mathcal{M}_p}{D_s} \frac{(c_2 - c_1) e^{\frac{U_L}{D_s}}}{c_2(e^{\frac{U_L}{D_s}} - 1)} \right], \tag{22}$$

where F(x) is

$$F(x) = \frac{(c_2 - c_1)e^{\frac{Ux}{D_s}} + c_1e^{\frac{UL}{D_s}} - c_2}{(1 + \frac{\mathcal{M}_p}{D_s})(c_2 - c_1)e^{\frac{Ux}{D_s}} + c_1e^{\frac{UL}{D_s}} - c_2}.$$
 (23)

These piecewise solutions are valid near the ends of the horizontal channel where the particle dynamics are relatively steady compared to the particle accumulation region within the channel. These solutions both diverge at  $x=x_p^\infty$ , i.e.,  $F(x_p^\infty)\to\infty$ , which is where the accumulation occurs [Fig. 10(d)]. The steady-state particle equilibrium location  $x_p^\infty$  reads

$$x_p^{\infty} = \frac{D_s}{U} \ln \left[ \frac{c_2 - c_1 e^{\frac{UL}{D_s}}}{(1 + \frac{M_p}{D_s})(c_2 - c_1)} \right]. \tag{24}$$

This equation provides the basis for diffusiophoresis separation in counter-gradient settings, which indicates that the particles with higher  $\mathcal{M}_d$  will accumulate more upstream so that mobility-based multiple particle sorting can be achieved [Fig. 10(e)].

Alternatively, Eq. (24) can be expressed as

$$\mathcal{M}_{p} = D_{s} \left[ \frac{c_{2} - c_{1} e^{\frac{UL}{D_{s}}}}{(c_{2} - c_{1}) e^{\frac{U_{s} \infty}{D_{s}}}} - 1 \right], \tag{25}$$

which can be useful for characterizing the colloid mobility by observing the equilibrium location. For a given particle  $(\mathcal{M}_d)$  and solute  $(D_s)$  pair, the particle equilibrium location  $x_p^\infty$  is determined by the solute transport, which is characterized by the solute Péclet number  $Pe_s$  and the solute contrast  $c_2/c_1$ . This is presented in Fig. 10(f), where the equilibrium position within the channel is shown as a function of  $Pe_s$  for varying  $\mathcal{M}_d/D_s$ .

Near the particle equilibrium location at which the particles build up over time due to the particle fluxes from both ends, the transient particle profile near the center peak is given as

$$n_c(x,t) = \alpha \cdot n_0 \frac{D_s t}{L^2} \exp \left[ -\frac{(D_s + \mathcal{M}_p)U^2}{2D_s D_p \mathcal{M}_p} (x - x_p^{\infty})^2 \right],$$
 (26)

where  $\alpha$  is given as

$$\alpha = \sqrt{\frac{1}{2\pi} \frac{\mathcal{M}_p}{D_p} \left( 1 + \frac{\mathcal{M}_p}{D_s} \right) \left( \frac{UL}{D_s} \right)^2 \frac{(c_2 - c_1)(c_2 - c_1 e^{\frac{UL}{D_s}})}{c_1 c_2 (e^{\frac{UL}{D_s}} - 1)}.$$
 (27)

Since the fluxes from both ends,  $\partial_x n_\ell|_0$  and  $\partial_x n_r|_L$ , are constant, the particles are expected to accumulate linearly in time. Practically, this prediction will become invalid once the particle density reaches the packing limit. The proportionality constant  $\alpha$  sets the particle accumulation rate, which is determined by the incoming particle fluxes from both ends and the particle back diffusion. Equation (26) along with Eqs. (21) and (22) describe the complete particle profile, which shows a good agreement with the full numerical calculation of Eqs. (9), (10), (12), and (13) [Fig. 10(d)].

### **B.** Experiments

## 1. Counter gradients by merging flow

Shin *et al.* demonstrated the counter-gradient diffusiophoresis using an H-shaped channel where two flow channels are bridged by a narrow pore [Fig. 11(a)]. <sup>79</sup> By flowing two solutions having different solutes and pressures through each channel, solute gradients are created within the pore, which is determined by the solute Péclet number across the pore [e.g., Eq. (20)]. Using polystyrene latex particles and NaCl gradients, the authors were able to visualize rapid particle accumulation within the pore [Fig. 11(b)]. The initial growth is shown to be linear in time, as also predicted theoretically in Eq. (26). The linear accumulation continues until the colloid reaches near the packing limit [Fig. 11(c)]. This effect is shown to be robust regardless of the particle or flow conditions provided that the solute concentrations are held constant at the flow junctions.

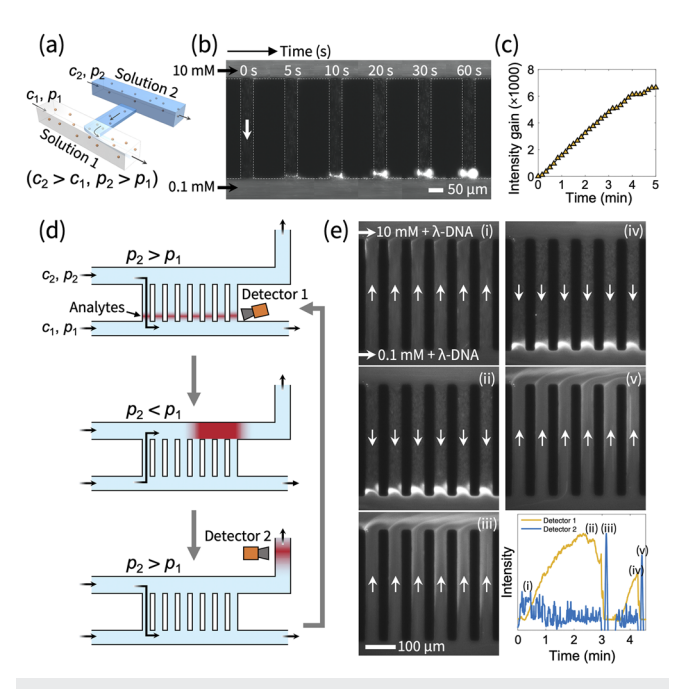
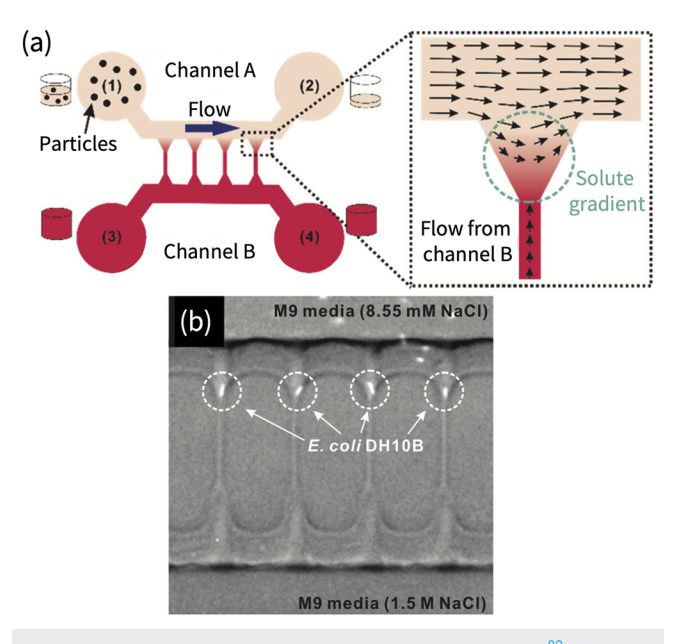


FIG. 11. Counter-gradient diffusiophoresis by merging flows in H-channels.<sup>79</sup> (a) Experimental setup. Two flow channels containing different solutions (c1 = 0.1 mM and  $c_2$  = 10 mM NaCl) are connected by a narrow pore. Pressure in the upper channel (solution 2) is larger than that in the lower channel (solution 1), so solution 2 advects through the pore and merges with solution 1, thus establishing solute gradients inside the pore. (b) Fluorescence image sequence of particles (PS,  $a = 0.25 \mu m$ ) accumulating near the bottom flow junction. (c) Evolution of the local maximum fluorescence intensity gain. (d) Repeatable preconcentrator for rapid bioassay. Upon pore flow, the dilute analytes are rapidly concentrated near the flow junctions, allowing stable detection in this region (detector 1). The accumulated analytes can be rapidly transferred to the other side of the channel by changing the pressure difference for mixing or flow-based detection in the downstream (detector 2). (e) Image sequence of repeated preconcentration and transfer of  $\lambda$ -DNAs. The plot indicates fluorescence intensity near the flow junction (detector 1) and downstream in the upper channel (detector 2). Reproduced with permission from Shin et al., "Accumulation of colloidal particles in flow junctions induced by fluid flow and diffusiophoresis," Phys. Rev. X 7, 041038 (2017). Copyright 2017 Author(s), licensed under a Creative Commons Attribution 4.0

Such a rapid, localized colloid accumulation can be particularly favorable for bioseparation, which involves preconcentration of analytes from dilute samples to overcome the detection limit of conventional analyzers. The authors utilized this phenomenon to achieve continuous, stationary bioseparation where they used a multiple array of pores to capture and deliver  $\lambda$ -DNAs on demand [Figs. 11(d) and 11(e)]. Due to its ability to accumulate at a fixed location, separation and detection can be made in a steady-state manner. Moreover, if the concentrated analytes require mixing with some other solution for subsequent analyses or require flow-based analysis, then the analytes can be passed onto the other side of the channel by controlling the channel pressure, allowing the analytes to be mixed and analyzed further downstream.

Hong *et al.* also used an H-shaped device to demonstrate single particle capturing at pore junction by counter-gradient diffusiophoresis (Fig. 12). Using a funnel-shaped junction made via hot embossing, the particles in flow stream (channel A) are brought closely to the junction, which exhibits strong solute gradients and relatively less advection [Fig. 12(a)]. Subsequently, nearby particles are drawn into the tight neck of the funnel by counter-gradient diffusiophoresis. Provided that the neck is narrow enough, the particles can be sieved and be locked in place. Using this approach, the authors were able to isolate individual bacterial cells (*E. coli*), which may be useful for single cell studies [Fig. 12(b)].



**FIG. 12.** Single cell capturing via counter-gradient diffusiophoresis. <sup>82</sup> (a) Experimental setup. H-shaped channels interfacing horizontal microfluidic channels and an array of vertical nanofluidic channels are created by hot embossing polymethyl methacrylate. Funnel-like junctions are formed [green dotted circle in the inset of (a)], which serve as localized regions to attract particles due to reduced cross-flow advection from channel A. (b) Captured individual *E. coli* in the funnel junctions. Both streams are M9 medium with NaCl concentration being 8.55 mM in the upper stream and 1.5M NaCl in the lower stream. Reproduced with permission from J. Hong, B. Kim, and H. Shin, "Mixed-scale poly(methyl methacrylate) channel network-based single-particle manipulation via diffusiophoresis," Nanoscale **10**, 14421–14431 (2018). Copyright 2018 Royal Society of Chemistry.

Instead of using H-shaped flow channels, Lee *et al.* demonstrated counter-gradient diffusiophoresis enabled by capillary imbibition. <sup>83</sup> By placing a porous Nafion membrane in contact with a microfluidic channel containing colloid suspension [Fig. 13(a)], bulk fluid flow in the suspension can be created toward the Nafion interface due to the imbibition, while the solute gradients are established simultaneously normal to the interface via cation exchange.

The imbibition dynamics can be controlled by modifying the shape of the Nafion medium such that the flow speed in the microfluidic channel changes over time [Fig. 13(b)]. Shaping the Nafion membrane into two sections of distinct cross-sectional areas thus results in a two-stage migration process. The initial stage preconcentrates the particles due to the counter-gradient diffusiophoresis enabled by the ion exchange process. During this stage, the particle velocity  $(U_{\mu})$  decays as  $t^{-1/2}$  due to the fluid flow and solute gradients generated by the straight Nafion section [Fig. 13(c)]. Once the fluid imbibes past the first straight section  $(t = t_c)$ , the

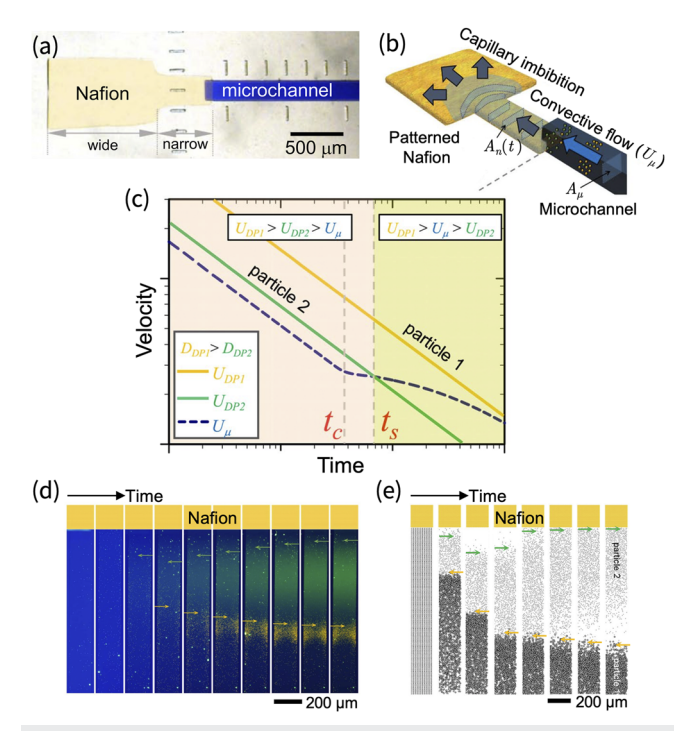


**FIG. 13.** Counter-gradient diffusiophoresis enabled by capillary imbibition in ion exchange membranes. <sup>83</sup> (a) Experimental setup. A porous ion exchange membrane (Nafion, yellow) is in contact with a straight microfluidic channel containing colloid suspension (blue). Solute gradients and fluid flow are created normal to the interface by cation exchange and capillary imbibition, respectively. (b) Nafion with varying cross-sectional area ( $A_n$ ) enables time-dependent control over fluid flow in the microfluidic channel. (c) Flow ( $U_\mu$ ) and particle diffusiophoretic velocity ( $U_{DP}$ ) change over time. Yellow curve indicates particles with high mobility (particle 1,  $U_{DP1}$ ) and the green curve indicates low mobility (particle 2,  $U_{DP2}$ ). (d) Experimental and (e) numerical demonstration of multiple particle separation [cPS, a = 20 nm (green arrows) and 1  $\mu$ m (yellow arrows)]. Reproduced with permission from Lee et al., "Spontaneous selective preconcentration leveraged by ion exchange and imbibition through nanoporous medium," Sci. Rep. 9, 2336 (2019). Copyright 2019 Author(s), licensed under a Creative Commons Attribution 4.0 License.

1D imbibition transitions to 2D such that the flow velocity decay deviates from the -1/2 power law, which enables the preconcentrated particles to separate depending on the particle mobility. The length of the straight section thus serves as a "timer" that sets the transition.

Such a time-dependent flow can be leveraged to allow certain particles to move in one direction and others in the opposite direction once the flow speed  $(U_{\mu})$  exceeds the diffusiophoretic speed  $(U_{DP})$  of the slower particle (which is when  $t > t_s$ ). As demonstrated experimentally [Fig. 13(d)] and computationally [Fig. 13(e)], the particles with low mobility move toward the interface (green arrows,  $U_{DP2}$ ), while the ones with high mobility move away from the interface (yellow arrows,  $U_{DP1}$ ), allowing simultaneous separation of multiple colloids. As the flow and the solute gradients are spontaneously created by porous Nafion, this approach may be a good candidate for portable, wireless diagnostics.

Recently, Rasmussen *et al.* reported the use of H-shaped devices for separating lipid vesicles. <sup>84</sup> Similar to previous studies, two streams containing different solute concentrations were injected through the main flow channels that run parallel [Fig. 14(a)]. However, instead of driving fluid flow across the connecting pores by pressure difference (e.g., Figs. 11 and 12), pore flow was induced chemically by diffusioosmotic slip flow. A unique feature is that tapered pores were introduced to control the pore flow. Contrary to straight pores in which the particle diffusiophoresis and wall

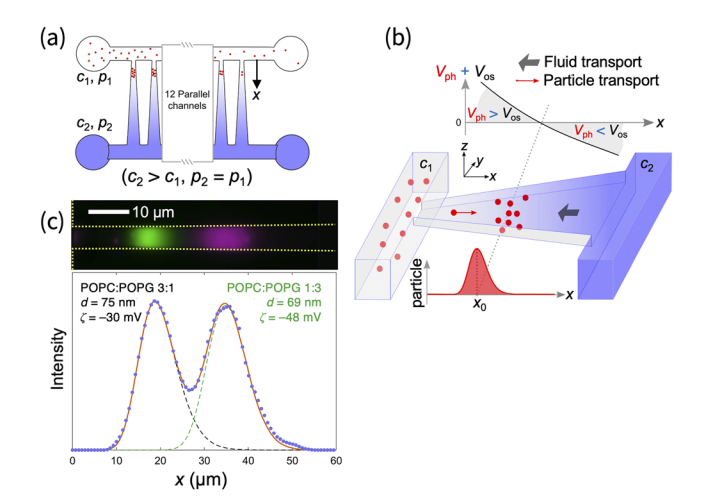
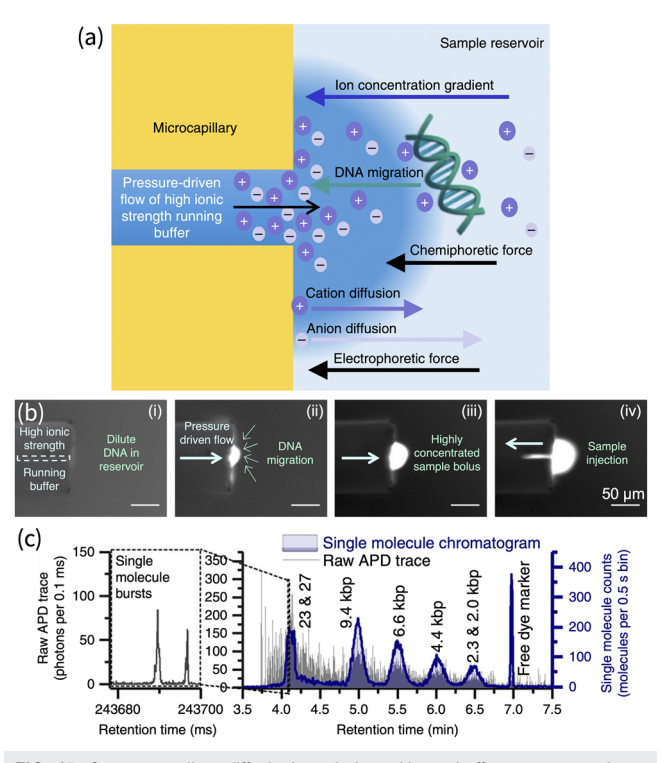


FIG. 14. Counter-gradient diffusiophoresis in tapered H-channels enabled by spatially varying diffusioosmosis.  $^{84}$  (a) Experimental setup. Flows containing different solute concentrations are injected through two large flow channels, and the tapered nanopores connect the two. Pressure is kept identical between the two flow channels ( $p_2 = p_1$ ). Due to the solute contrast ( $c_2 > c_1$ ), fluid advection in the pores is induced solely by diffusioosmosis. (b) The tapered pores induce diffusioosmotic pore flow ( $V_{os}$ ) that exhibits distinct solute dependence compared to the particle diffusiophoresis ( $V_{ph}$ ). This results in a crossover between the two velocities in the pore, enabling stationary particle accumulation. (c) Separation of phospholipid vesicles from a mixture.  $c_1 = 0.003 \times$  and  $c_2 = 10 \times$  phosphate-buffered saline (PBS). Reproduced with permission from M. K. Rasmussen, J. N. Pedersen, and R. Marie, "Size and surface charge characterization of nanoparticles with a salt gradient," Nat. Commun. 11, 2337 (2020). Copyright 2020 Author(s), licensed under a Creative Commons Attribution 4.0 License.

diffusioosmosis both follow the same functional dependence on the solute concentration, the tapered pores induce diffusioosmotic pore flow ( $V_{\rm os}$ ) that exhibits different solute dependence compared to the particle diffusiophoresis ( $V_{\rm ph}$ ). Consequently, a crossover between the two velocities is introduced, enabling stationary particle accumulation [Fig. 14(b)]. By exploiting the mobility-dependent colloid accumulation, the authors were able to separate vesicles from a mixture of vesicles with different mobilities, analogous to previous demonstrations in other settings.  $^{73,79,80,83}$ 

# 2. Counter gradients by radial diffusion

An alternative way of achieving counter-gradient diffusiophoresis is by connecting a narrow channel to a large stagnant reservoir such that a solution flowing through the channel exits into the reservoir containing different solution [Fig. 10(b)]. Due to the radial diffusion taking place in the reservoir near the channel exit, a



**FIG. 15.** Counter-gradient diffusiophoresis by exiting a buffer stream to a large reservoir containing different solution. <sup>85</sup> (a) Schematic illustration of DNA preconcentration using counter-gradient diffusiophoresis. Pressure-driven flow drives the running buffer with high ionic strength out of the capillary into the reservoir buffer with low ionic strength. This creates radial solute gradients surrounding the capillary orifice, leading to particle diffusiophoresis and accumulation. (b) DNA preconcentration and subsequent reinjection into the capillary by counter-gradient diffusiophoresis. (c) Separation and detection of a mixture of  $\lambda$ -DNAs with various sizes enabled by interfacing diffusiophoretic preconcentration, hydrodynamic separation, and single-molecule detection platform. Reproduced with permission from Friedrich *et al.*, "Molecular rheotaxis directs DNA migration and concentration against a pressure-driven flow," Nat. Commun. **8**, 1213 (2017). Copyright 2017 Author(s), licensed under a Creative Commons Attribution 4.0 License.

steady-state concentration profile can be expected, allowing localized particle accumulation. Friedrich et al. demonstrated this concept to achieve preconcentration and separation of  $\lambda$ -DNAs [Fig. 15(a)]. 85 A thin glass capillary was connected to an analyte reservoir containing DNAs. By flowing buffer solution through the capillary, the charged DNA molecules present in the reservoir migrated toward the capillary and eventually accumulated at the equilibrium position [Fig. 15(b)]. Similar to H-shaped channels, the DNA accumulation was also shown to be linear in time. Through buffer optimization, the authors were able to achieve over 10 000-fold increase in the DNA concentration in 45 min. Once accumulated, the DNA molecules are injected back into the capillary for chromatography [Fig. 15(b); right panel]. By interfacing this method with hydrodynamic separation and single molecule sensing, the authors were able to demonstrate simultaneous separation and detection of multiple DNAs from a single batch [Fig. 15(c)].

Some distinct advantages of this method exist over the merging flow streams in H-shaped channels: (1) this method is free from undesired diffusioosmosis since the accumulation takes place outside of the capillary, which may otherwise disperse the concentrated analytes, and (2) preconcentration can be achieved with a single flow control system, whereas H-shaped channels require flow control of two separate channels.

Using the similar method, Li *et al.* recently demonstrated DNA preconcentration in high ionic strength, <sup>86</sup> which is often unfeasible in electrokinetic assays. Such a demonstration shows its utility in practical biomedical applications where analytes are typically suspended in physiological solutions containing a mixture of concentrated solutes.

## V. CONCLUSION AND OUTLOOK

Recent developments in diffusiophoretic colloid separation have proven its potential for continuous separation, particularly for applications that require portability and a small sample size. Nevertheless, certain limitations exist in diffusiophoretic separation such as the mixing of unwanted chemicals or the need for a relatively large solute contrast and particle surface charge to meet the practical separation performance. Most of the literature covered in this review are proof-of-concept studies where further investigations are needed to achieve separation systems that can compete with existing methods.

Other new ideas may also stem from the previous studies covered in this review. For instance, the photocatalytic particles from the work of Visan and Lammertink can serve as a mobile, localized solute source that may induce diffusiophoresis of other passive particles on demand, which is analogous to "mobile solutal beacons" demonstrated by Banerjee *et al.* recently [Fig. 16(a)].<sup>87</sup> One can also exploit the logarithmic dependence of diffusiophoresis (i.e.,  $u_d \sim \nabla \ln c$ ) for enhancing the separation efficacy by imposing alternating cross gradients. As previously demonstrated by Palacci *et al.*, <sup>21</sup> periodic solute gradients can effectively segregate charged colloidal particles due to the asymmetric particle motion induced by the logarithmic dependence [Fig. 16(b)]. Thus, imposing alternating solute gradients, either spatially or temporally, along the downstream may further enhance separation in cross-gradient diffusiophoresis systems.

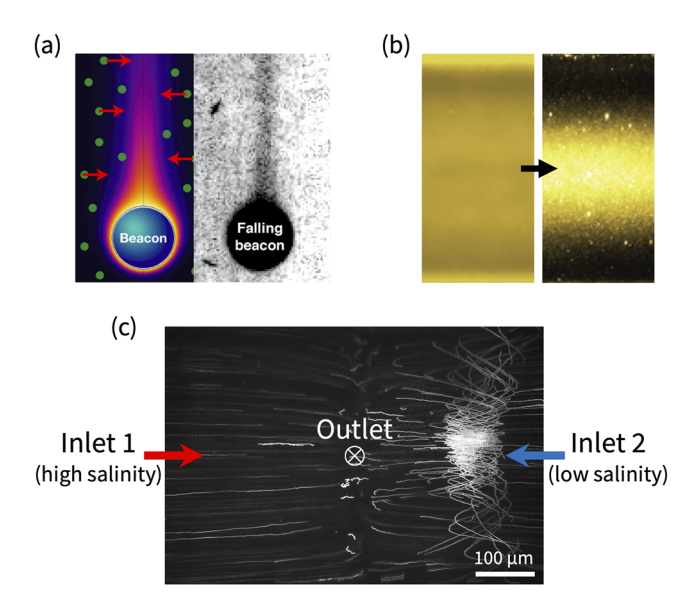


FIG. 16. Some recent works that may inspire new developments in diffusiophoretic separation. (a) A falling solutal beacon leaves behind a trace of solutes that attracts passive particles via diffusiophoresis.<sup>87</sup> (b) Imposing periodic solute gradients on the boundaries can enhance particle segregation.<sup>21</sup> (c) Particle trapping in the merging T-junction with salinity contrast by diffusioosmotic vortices.<sup>88</sup> The vortex occurs due to the interplay between out-of-plane diffusiophoresis and in-plane diffusioosmosis. (a) is reproduced with permission from A. Banerjee, H. Tan, and T. M. Squires, "Drop-in additives for suspension manipulation: Colloidal motion induced by sedimenting soluto-inertial beacons," Phys. Rev. Fluids 5, 073701 (2020). Copyright 2020 American Physical Society. (b) is reproduced with permission from Palacci et al., "Colloidal motility and pattern formation under rectified diffusiophoresis," Phys. Rev. Lett. 104, 138302 (2010). Copyright 2010 American Physical Society. (c) is reproduced with permission from Shin et al., "Particle trapping in merging flow junctions by fluid-solute-colloid-boundary interactions," Phys. Rev. Fluids 5, 024304 (2020). Copyright 2020 Author(s), licensed under a Creative Commons Attribution 4.0 License.

Also, this review largely neglects diffusioosmosis, which is often considered as a higher-order effect in flow systems. However, there are many examples in which diffusioosmosis plays a major role in colloid dynamics in the presence of background flow such as the drying of sessile colloidal drops, <sup>89</sup> the mixing of colloidal suspensions in merging flow junctions, <sup>88</sup> and particle entry and trapping in confined spaces. <sup>90,91</sup> Further examples regarding useful applications enabled by diffusioosmosis include liquid pumping, <sup>80</sup> surface characterization, <sup>92–94</sup> enhanced slip, <sup>95</sup> nanopore DNA sensing, <sup>22,96</sup> and oil recovery. <sup>30</sup> As diffusioosmosis occurs only along the surface gradient of the solute concentration [i.e.,  $u \sim (I - nn) \cdot \nabla \ln c$ ], exploiting diffusioosmosis in complex flow geometries where diffusioosmosis and diffusiophoresis are not necessarily parallel to each other [Fig. 16(c); see Ref. 88] may invoke richer particle dynamics that may lead to unprecedented separation strategies.

### **ACKNOWLEDGMENTS**

This material is based upon work supported by the National Science Foundation under Grant No. CBET-1930691. The author thanks Jesse Ault and Viet Sang Doan for valuable feedback.

#### **DATA AVAILABILITY**

The data that support the findings of this study are available from the corresponding author upon reasonable request.

#### REFERENCES

- <sup>1</sup>A. Lenshof and T. Laurell, "Continuous separation of cells and particles in microfluidic systems," Chem. Soc. Rev. **39**, 1203–1217 (2010).
- <sup>2</sup>P. Sajeesh and A. K. Sen, "Particle separation and sorting in microfluidic devices: A review," Microfluid. Nanofluid. 17, 1–52 (2014).
- <sup>3</sup>T. Akagi and T. Ichiki, "Cell electrophoresis on a chip: What can we know from the changes in electrophoretic mobility?," Anal. Bioanal. Chem. **391**, 2433 (2008).
- <sup>4</sup>N. Pamme and A. Manz, "On-chip free-flow magnetophoresis: Continuous flow separation of magnetic particles and agglomerates," Anal. Chem. **76**, 7250–7256 (2004).
- <sup>5</sup>P. R. C. Gascoyne and J. Vykoukal, "Particle separation by dielectrophoresis," Electrophoresis **23**, 1973 (2002).
- <sup>6</sup>D. Vigolo, R. Rusconi, H. A. Stone, and R. Piazza, "Thermophoresis: Microfluidics characterization and separation," Soft Matter 6, 3489–3493 (2010).
- <sup>7</sup>G. K. Kurup and A. S. Basu, "Tensiophoresis: Migration and sorting of droplets in an interfacial tension gradient," in *15th International Conference on Miniaturized Systems for Chemistry and Life Sciences (MicroTAS 2011)* (Royal Society of Chemistry, 2011), pp. 1367–1369.
- <sup>8</sup>B. Abécassis, C. Cottin-Bizonne, C. Ybert, A. Ajdari, and L. Bocquet, "Boosting migration of large particles by solute contrasts," Nat. Mater. 7, 785–789 (2008).
- <sup>9</sup>F. Petersson, L. Åberg, A.-M. Swärd-Nilsson, and T. Laurell, "Free flow acoustophoresis: Microfluidic-based mode of particle and cell separation," Anal. Chem. **79**, 5117–5123 (2007).
- <sup>10</sup>M. P. MacDonald, G. C. Spalding, and K. Dholakia, "Microfluidic sorting in an optical lattice," Nature 426, 421 (2003).
- <sup>11</sup>D. Di Carlo, "Inertial microfluidics," Lab Chip **9**, 3038–3046 (2009).
- <sup>12</sup>B. V. Derjaguin, G. P. Sidorenkov, E. A. Zubashchenkov, and E. V. Kiseleva, "Kinetic phenomena in boundary films of liquids," Kolloidn. Zh. 9, 335–347 (1947)
- <sup>13</sup>D. C. Prieve, J. L. Anderson, J. P. Ebel, and M. E. Lowell, "Motion of a particle generated by chemical gradients. Part 2. Electrolytes," J. Fluid Mech. 148, 247–269 (1984).
- <sup>14</sup>J. L. Anderson and D. C. Prieve, "Diffusiophoresis: Migration of colloidal particles in gradients of solute concentration," Sep. Purif. Methods 13, 67–103 (1984).
- <sup>15</sup> J. L. Moran and J. D. Posner, "Phoretic self-propulsion," Annu. Rev. Fluid Mech. 49, 511–540 (2017).
- <sup>16</sup>G. Gompper, R. G. Winkler, T. Speck, A. Solon, C. Nardini, F. Peruani, H. Löwen, R. Golestanian, U. B. Kaupp, L. Alvarez et al., "The 2020 motile active matter roadmap," J. Phys.: Condens. Matter 32, 193001 (2020).
- <sup>17</sup>Z. Lu, M. H. K. Schaarsberg, X. Zhu, L. Y. Yeo, D. Lohse, and X. Zhang, "Universal nanodroplet branches from confining the Ouzo effect," Proc. Natl. Acad. Sci. U. S. A. 114, 10332–10337 (2017).
- <sup>18</sup> F. Yang, S. Shin, and H. A. Stone, "Diffusiophoresis of a charged drop," J. Fluid Mech. 852, 37–59 (2018).
- <sup>19</sup>O. Annunziata, D. Buzatu, and J. G. Albright, "Protein diffusiophoresis and salt osmotic diffusion in aqueous solutions," J. Phys. Chem. B **116**(42), 12694–12705 (2012)
- <sup>20</sup>A. Fahim and O. Annunziata, "Amplification of salt-induced protein diffusiophoresis by varying salt from potassium to sodium to magnesium chloride in water," Langmuir 36, 2635–2643 (2020).
- <sup>21</sup> J. Palacci, B. Abecassis, C. Cottin-Bizonne, C. Ybert, and L. Bocquet, "Colloidal motility and pattern formation under rectified diffusiophoresis," Phys. Rev. Lett. 104, 138302 (2010).
- <sup>22</sup> A. McMullen, G. Araujo, M. Winter, and D. Stein, "Osmotically driven and detected DNA translocations," Sci. Rep. 9, 15065 (2019).
- <sup>23</sup>S. V. Hartman, B. Bozic, and J. Derganc, "Migration of blood cells and phospholipid vesicles induced by concentration gradients in microcavities," New Biotechnol. 47, 60–66 (2018).

- <sup>24</sup>V. S. Doan, P. Saingam, T. Yan, and S. Shin, "A trace amount of surfactants enables diffusiophoretic swimming of bacteria," ACS Nano (in press)
- <sup>25</sup> A. Kodama, Y. Sakuma, M. Imai, T. Kawakatsu, N. Puff, and M. I. Angelova, "Migration of phospholipid vesicles can be selectively driven by concentration gradients of metal chloride solutions," Langmuir 33, 10698-10706 (2017).
- <sup>26</sup>S. Shin, V. S. Doan, and J. Feng, "Osmotic delivery and release of lipidencapsulated molecules via sequential solution exchange," Phys. Rev. Appl. 12, 024014 (2019).
- <sup>27</sup>J. L. Anderson, "Colloid transport by interfacial forces," Annu. Rev. Fluid Mech. 21, 61-99 (1989).
- <sup>28</sup>D. Velegol, A. Garg, R. Guha, A. Kar, and M. Kumar, "Origins of concentration gradients for diffusiophoresis," Soft Matter 12, 4686–4703 (2016).
- H. J. Keh, "Diffusiophoresis of charged particles and diffusioosmosis of electrolyte solutions," Curr. Opin. Colloid Interface Sci. 24, 13-22 (2016).
- 30 S. Marbach and L. Bocquet, "Osmosis, from molecular insights to large-scale
- applications," Chem. Soc. Rev. 48, 3102 (2019).
  <sup>31</sup> R. P. Sear and P. B. Warren, "Diffusiophoresis in nonadsorbing polymer solutions: The Asakura-Oosawa model and stratification in drying films," Phys. Rev. E 96, 062602 (2017).
- <sup>32</sup>O. E. Shklyaev, H. Shum, and A. C. Balazs, "Using chemical pumps and motors to design flows for directed particle assembly," Acc. Chem. Res. 51, 2672-2680
- 33 R. Guha, X. Shang, A. L. Zydney, D. Velegol, and M. Kumar, "Diffusiophoresis contributes significantly to colloidal fouling in low salinity reverse osmosis systems," J. Membr. Sci. 479, 67-76 (2015).
- <sup>34</sup>S. Shin, P. B. Warren, and H. A. Stone, "Cleaning by surfactant gradients: Particulate removal from porous materials and the significance of rinsing in laundry detergency," Phys. Rev. Appl. 9, 034012 (2018).
- 35 V. Yadav, J. D. Freedman, M. Grinstaff, and A. Sen, "Bone-crack detection, targeting, and repair using ion gradients," Angew. Chem., Int. Ed. 52, 10997-11001 (2013).
- <sup>36</sup>R. P. Sear, "Diffusiophoresis in cells: A general nonequilibrium, nonmotor mechanism for the metabolism-dependent transport of particles in cells," Phys. Rev. Lett. 122, 128101 (2019).
- <sup>37</sup>B. Ramm, A. Goychuk, A. Khmelinskaia, P. Blumhardt, K. A. Ganzinger, E. Frey, and P. Schwille, "ATP driven diffusiophoresis: Active cargo transport without motor proteins," bioRxiv:072744 (2020).
- 38 F. M. Möller, F. Kriegel, M. Kiess, V. Sojo, and D. Braun, "Steep pH gradients and directed colloid transport in a microfluidic alkaline hydrothermal pore," Angew. Chem., Int. Ed. 56, 2340-2344 (2017).
- $^{39}$  J. C. Giddings, "Field-flow fractionation: Analysis of macromolecular, colloidal, and particulate materials," Science 260, 1456-1465 (1993).
- <sup>40</sup>C. W. Shields IV, C. D. Reyes, and G. P. López, "Microfluidic cell sorting: A review of the advances in the separation of cells from debulking to rare cell isolation," Lab Chip 15, 1230-1249 (2015).
- <sup>41</sup>S. Duhr and D. Braun, "Optothermal molecule trapping by opposing fluid flow with thermophoretic drift," Phys. Rev. Lett. 97, 038103 (2006).
- <sup>42</sup>D. Stein, Z. Deurvorst, F. H. J. van der Heyden, W. J. A. Koopmans, A. Gabel, and C. Dekker, "Electrokinetic concentration of DNA polymers in nanofluidic channels," Nano Lett. 10, 765-772 (2010).
- <sup>43</sup>R. F. Probstein, *Physicochemical Hydrodynamics: An Introduction* (John Wiley & Sons, 2005).
- 44T.-Y. Chiang and D. Velegol, "Multi-ion diffusiophoresis," J. Colloid Interface Sci. 424, 120-123 (2014).
- $^{\bf 45}$  A. Gupta, B. Rallabandi, and H. A. Stone, "Diffusiophoretic and diffusioosmotic velocities for mixtures of valence-asymmetric electrolytes," Phys. Rev. Fluids 4, 043702 (2019).
- <sup>46</sup>H. J. Keh and Y. K. Wei, "Diffusiophoretic mobility of spherical particles at low potential and arbitrary double-layer thickness," Langmuir 16, 5289-5294
- <sup>47</sup>J. H. Masliyah, *Electrokinetic Transport Phenomena* (Alberta Oil Sands Technology and Research Authority, Edmonton, 1994).
- <sup>48</sup>S. Marbach, H. Yoshida, and L. Bocquet, "Local and global force balance for diffusiophoretic transport," J. Fluid Mech. 892, A6 (2020).

- <sup>49</sup>D. Long, J.-L. Viovy, and A. Ajdari, "Simultaneous action of electric fields and nonelectric forces on a polyelectrolyte: Motion and deformation," Phys. Rev. Lett. 76, 3858 (1996).
- $^{\bf 50}$  J. P. Brody, P. Yager, R. E. Goldstein, and R. H. Austin, "Biotechnology at low Reynolds numbers," Biophys. J. 71, 3430-3441 (1996).
- <sup>51</sup> A. Hatch, A. E. Kamholz, K. R. Hawkins, M. S. Munson, E. A. Schilling, B. H. Weigl, and P. Yager, "A rapid diffusion immunoassay in a T-sensor," N Biotechnol. 19, 461-465 (2001).
- 52 K. Lee, J. Lee, D. Ha, M. Kim, and T. Kim, "Low-electric-potential-assisted diffusiophoresis for continuous separation of nanoparticles on a chip," Lab Chip 20, 2735-2747 (2020).
- 53 S. Shin, O. Shardt, P. B. Warren, and H. A. Stone, "Membraneless water filtration using CO<sub>2</sub>," Nat. Commun. 8, 15181 (2017).
- <sup>54</sup>T. J. Shimokusu, V. G. Maybruck, J. T. Ault, and S. Shin, "Colloid separation by CO<sub>2</sub>-induced diffusiophoresis," Langmuir 36, 7032-7038 (2020).
- 55 H. Lee, J. Kim, J. Yang, S. W. Seo, and S. J. Kim, "Diffusiophoretic exclusion of colloidal particles for continuous water purification," Lab Chip 18, 1713-1724
- 56 A. Visan and R. G. Lammertink, "Reaction induced diffusiophoresis of ordinary catalytic particles," React. Chem. Eng. 4, 1439-1446 (2019).
- <sup>57</sup>J.-B. Salmon and A. Ajdari, "Transverse transport of solutes between co-flowing pressure-driven streams for microfluidic studies of diffusion/reaction processes,' J. Appl. Phys. 101, 074902 (2007).
- 58 R. F. Ismagilov, A. D. Stroock, P. J. A. Kenis, G. M. Whitesides, and H. A. Stone, "Experimental and theoretical scaling laws for transverse diffusive broadening in two-phase laminar flows in microchannels," Appl. Phys. Lett. 76, 2376-2378
- <sup>59</sup>P. O. Staffeld and J. A. Quinn, "Diffusion-induced banding of colloid particles via diffusiophoresis: 1. Electrolytes," J. Colloid Interface Sci. 130, 69-87 (1989).
- <sup>60</sup>B. Abécassis, C. Cottin-Bizonne, C. Ybert, A. Ajdari, and L. Bocquet, "Osmotic manipulation of particles for microfluidic applications," New J. Phys. 11, 075022
- <sup>61</sup> J. Palacci, S. Sacanna, A. P. Steinberg, D. J. Pine, and P. M. Chaikin, "Living crystals of light-activated colloidal surfers," Science 339, 936-940 (2013).
- 62 F. Yang, B. Rallabandi, and H. A. Stone, "Autophoresis of two adsorbing/desorbing particles in an electrolyte solution," J. Fluid Mech. 865, 440-459 (2019).
- 63 S.-Y. Cheng, S. Heilman, M. Wasserman, S. Archer, M. L. Shuler, and M. Wu, "A hydrogel-based microfluidic device for the studies of directed cell migration," Lab Chip 7, 763-769 (2007).
- <sup>64</sup>T. Ahmed, T. S. Shimizu, and R. Stocker, "Bacterial chemotaxis in linear and nonlinear steady microfluidic gradients," Nano Lett. 10, 3379-3385 (2010).
- <sup>65</sup>J. S. Paustian, C. D. Angulo, R. Nery-Azevedo, N. Shi, A. I. Abdel-Fattah, and T. M. Squires, "Direct measurements of colloidal solvophoresis under imposed solvent and solute gradients," Langmuir 31, 4402-4410 (2015).
- <sup>66</sup>T. C. Merkel, V. I. Bondar, K. Nagai, B. D. Freeman, and I. Pinnau, "Gas sorption, diffusion, and permeation in poly(dimethylsiloxane)," J. Polym. Sci., Part B: Polym. Phys. 38, 415-434 (2000).
- <sup>67</sup>E. Blanco, H. Shen, and M. Ferrari, "Principles of nanoparticle design for overcoming biological barriers to drug delivery," Nat. Biotechnol. 33, 941
- <sup>68</sup>Y. Zhu, D. Wang, L. Jiang, and J. Jin, "Recent progress in developing advanced membranes for emulsified oil/water separation," NPG Asia Mater. 6, e101
- <sup>69</sup> J. Ran, L. Wu, Y. He, Z. Yang, Y. Wang, C. Jiang, L. Ge, E. Bakangura, and T. Xu, "Ion exchange membranes: New developments and applications," J. Membr. Sci. 522, 267-291 (2017).
- ${\bf ^{70}}$  D. Florea, S. Musa, J. M. Huyghe, and H. M. Wyss, "Long-range repulsion of colloids driven by ion exchange and diffusiophoresis," Proc. Natl. Acad. Sci. U. S. A. 111, 6554-6559 (2014).
- <sup>71</sup> J. J. McDermott, A. Kar, M. Daher, S. Klara, G. Wang, A. Sen, and D. Velegol, "Self-generated diffusioosmotic flows from calcium carbonate micropumps," Langmuir 28, 15491-15497 (2012).
- 72 A. Kar, T.-Y. Chiang, I. O. Rivera, A. Sen, and D. Velegol, "Enhanced transport into and out of dead-end pores," ACS Nano 9, 746-753 (2015).

- <sup>73</sup>S. Shin, E. Um, B. Sabass, J. T. Ault, M. Rahimi, P. B. Warren, and H. A. Stone, "Size-dependent control of colloid transport via solute gradients in dead-end channels," Proc. Natl. Acad. Sci. U. S. A. 113, 257–261 (2016).
- <sup>74</sup> A. Banerjee, I. Williams, R. N. Azevedo, M. E. Helgeson, and T. M. Squires, "Soluto-inertial phenomena: Designing long-range, long-lasting, surface-specific interactions in suspensions," Proc. Natl. Acad. Sci. U. S. A. 113, 8612–8617 (2016).
  <sup>75</sup> N. Shi, R. Nery-Azevedo, A. I. Abdel-Fattah, and T. M. Squires, "Diffusio-
- phoretic focusing of suspended colloids," Phys. Rev. Lett. 117, 258001 (2016).

  76 F. Boulogne, S. Shin, J. Dervaux, L. Limat, and H. A. Stone, "Diffusiophoretic
- <sup>76</sup>F. Boulogne, S. Shin, J. Dervaux, L. Limat, and H. A. Stone, "Diffusiophoretic manipulation of particles in a drop deposited on a hydrogel," Soft Matter 13, 5122–5129 (2017).
- <sup>77</sup>D. Ha, S. Seo, K. Lee, and T. Kim, "Dynamic transport control of colloidal particles by repeatable active switching of solute gradients," ACS Nano 13, 12939–12948 (2019).
- <sup>78</sup> A. Banerjee and T. M. Squires, "Long-range, selective, on-demand suspension interactions: Combining and triggering soluto-inertial beacons," Sci. Adv. 5, eaax1893 (2019).
- <sup>79</sup>S. Shin, J. T. Ault, P. B. Warren, and H. A. Stone, "Accumulation of colloidal particles in flow junctions induced by fluid flow and diffusiophoresis," Phys. Rev. X 7, 041038 (2017).
- <sup>80</sup> J. T. Ault, S. Shin, and H. A. Stone, "Diffusiophoresis in narrow channel flows," J. Fluid Mech. 854, 420–448 (2018).
- <sup>81</sup>S. J. Kim, Y.-A. Song, and J. Han, "Nanofluidic concentration devices for biomolecules utilizing ion concentration polarization: Theory, fabrication, and applications," Chem. Soc. Rev. 39, 912–922 (2010).
- <sup>82</sup>J. Hong, B. Kim, and H. Shin, "Mixed-scale poly(methyl methacrylate) channel network-based single-particle manipulation via diffusiophoresis," Nanoscale 10, 14421–14431 (2018).
- <sup>83</sup>D. Lee, J. A. Lee, H. Lee, and S. J. Kim, "Spontaneous selective preconcentration leveraged by ion exchange and imbibition through nanoporous medium," Sci. Rep. 9, 2336 (2019).
- <sup>84</sup>M. K. Rasmussen, J. N. Pedersen, and R. Marie, "Size and surface charge characterization of nanoparticles with a salt gradient," Nat. Commun. 11, 2337 (2020).

- <sup>85</sup>S. M. Friedrich, J. M. Burke, K. J. Liu, C. F. Ivory, and T.-H. Wang, "Molecular rheotaxis directs DNA migration and concentration against a pressure-driven flow," Nat. Commun. **8**, 1213 (2017).
- <sup>86</sup>S. Li, A. Li, K. Hsieh, S. M. Friedrich, and T.-H. Wang, "Electrode-free concentration and recovery of DNA at physiologically relevant ionic concentrations," Anal. Chem. 92, 6150–6157 (2020).
- <sup>87</sup> A. Banerjee, H. Tan, and T. M. Squires, "Drop-in additives for suspension manipulation: Colloidal motion induced by sedimenting soluto-inertial beacons," Phys. Rev. Fluids 5, 073701 (2020).
- <sup>88</sup>S. Shin, J. T. Ault, K. Toda-Peters, and A. Q. Shen, "Particle trapping in merging flow junctions by fluid-solute-colloid-boundary interactions," Phys. Rev. Fluids **5**, 024304 (2020).
- <sup>89</sup>R. Guha, F. Mohajerani, A. Mukhopadhyay, M. D. Collins, A. Sen, and D. Velegol, "Modulation of spatiotemporal particle patterning in evaporating droplets: Applications to diagnostics and materials science," ACS Appl. Mater. Interfaces 9, 43352–43362 (2017).
- <sup>90</sup>S. Battat, J. T. Ault, S. Shin, S. Khodaparast, and H. A. Stone, "Particle entrainment in dead-end pores by diffusiophoresis," Soft Matter 15, 3879–3885 (2019).
- <sup>91</sup>N. Singh, G. T. Vladisavljevic, F. Nadal, C. Cottin-Bizonne, C. Pirat, and G. Bolognesi, "Reversible trapping of colloids in microgrooved channels via steady-state solute gradients," arXiv:2007.11114 [cond-mat.soft] (2020).
- <sup>92</sup>C. Lee, C. Cottin-Bizonne, A. L. Biance, P. Joseph, L. Bocquet, and C. Ybert, "Osmotic flow through fully permeable nanochannels," Phys. Rev. Lett. 112, 244501 (2014).
- <sup>93</sup>S. Shin, J. T. Ault, J. Feng, P. B. Warren, and H. A. Stone, "Low-cost zeta potentiometry using solute gradients," Adv. Mater. 29, 1701516 (2017).
- <sup>94</sup>J. T. Ault, S. Shin, and H. A. Stone, "Characterization of surface-solute interactions by diffusioosmosis," Soft Matter **15**, 1582–1596 (2019).
- <sup>95</sup> A. Ajdari and L. Bocquet, "Giant amplification of interfacially driven transport by hydrodynamic slip: Diffusio-osmosis and beyond," Phys. Rev. Lett. **96**, 186102 (2006).
- <sup>96</sup>M. M. Hatlo, D. Panja, and R. van Roij, "Translocation of DNA molecules through nanopores with salt gradients: The role of osmotic flow," Phys. Rev. Lett. 107, 068101 (2011).